

# Impacts of subgrid elevation bands on hydrological portrayals: insights from a suite of hydroclimatically diverse mountainous catchments

Octavio Murillo<sup>1</sup>, Pablo A. Mendoza<sup>1,2</sup>, Nicolás Vásquez<sup>1</sup>, Naoki Mizukami<sup>3</sup> and Álvaro Ayala<sup>4</sup>

<sup>1</sup>Department of Civil Engineering, Universidad de Chile, Santiago, Chile.

<sup>2</sup>Advanced Mining Technology Center (AMTC), Universidad de Chile, Santiago, Chile.

<sup>3</sup>National Center for Atmospheric Research (NCAR), Boulder, Colorado, USA.

<sup>4</sup>Centro de Estudios Avanzados en Zonas Áridas (CEAZA), La Serena, Chile.

Corresponding author: Pablo Mendoza ([pamendoz@uchile.cl](mailto:pamendoz@uchile.cl))

**Keywords:** Elevation bands, vertical discretization, VIC, spatial heterogeneity, snow water equivalent

## Key Points:

- Elevation bands do not affect basin-scale runoff considerably, but they perturb other hydrological fluxes and their spatial variability.
- Simulated peak SWE is more affected by elevation bands in dry periods, and such effects are not proportional to vertical discretization.
- Elevation bands are important in grid cells with relatively low altitude, high elevation ranges, steep slopes and pronounced seasonality.

## Abstract

The implementation of elevation bands is a common strategy to account for vertical heterogeneity in hydrology and land surface models; however, there is no consensus guidelines for their delineation. We characterize hydrological implications of this choice by configuring the Variable Infiltration Capacity (VIC) model in nine mountainous basins of the Andes Cordillera, central Chile, using six different setups: no elevation bands (benchmark model), and elevation bands with vertical discretizations of 1000, 750, 500, 200 and 100 m. The analyses are conducted in a wet period (April/1982-March/1987), dry period (April/2010-March/2015) and a climatological period (April/1982-March/2015). The results show that adding elevation bands yield little variations in simulated monthly or daily streamflow; however, there are important effects on the partitioning of precipitation between snowfall and rainfall, snowmelt, sublimation, and the spatial variability in September 1 SWE, suggesting a model-structure equifinality. Incorporating elevation bands generally yields less basin-averaged snowmelt, and more (less) catchment-scale sublimation across water-limited (energy-limited) basins. Further, the implications of elevation bands vary with the analysis period: fluxes are more affected during the wet period, while variations in September 1 SWE are more noticeable during the dry period. In general, the effects of adding elevation bands are reduced with increasing vertical discretization, and can differ among catchments. Finally, the grid cells that yield the largest sensitivities to vertical discretization have relatively lower mean altitude, elevation ranges  $>1000$  m, steep slopes ( $>15^\circ$ ) and annual precipitation amounts  $<1000$  mm, with large intra-annual variations in the water/energy budget.

## Plain Language Summary

Spatially distributed computer-based models are widely used to make predictions on water availability. In mountainous areas, it is common to use elevation bands to represent complex topography within each modeling unit in a simplified manner; however, the effects of the selected number of bands and/or elevation range on model results have not been assessed in detail. We use a suite of diverse Andean basins to document how the configuration of elevation bands affect the simulation of the water cycle at different spatial scales. Our results show that, although the incorporation of elevation bands has little effects on the simulation of discharge at the basin outlets, similar results can arise from different spatial distributions of rainfall, snowfall, snowmelt, sublimation and maximum annual accumulation. The implications of adding elevation bands may vary with the climate conditions (i.e., wet/dry) of the analysis period. Finally, we identify mean altitude, elevation range, slope and annual precipitation as the variables that should be examined carefully to decide where (i.e., which grid cells) the choice of elevation band configuration should be made with more caution.

## 1 Introduction

Snow is essential for water supply in mountain environments. In this context, numerical models are not only useful for understanding the physical processes that determine snow accumulation and melting (Liston & Sturm, 1998; Lehning et al., 2006; Clark et al., 2017), but also to make predictions that can be used for decision making (Schneider & Molotch, 2016), especially considering ongoing and future changes in climatic conditions (IPCC, 2021). Indeed, climate change is expected to impact mountain snowpack in many mountain regions of the world (Barnett et al., 2005), such as the Colorado Headwaters of USA (Rasmussen et al., 2014), the Appalachian Mountains (Demaria et al., 2016), the eastern Himalayas of Nepal (Bhatta et al.,

2019), the extratropical Andes (Vicuña et al., 2021), and the Spanish Pyrenees (López-Moreno et al., 2013). Hence, improving the realism of snow models is critical for reliable estimates of snow water equivalent (SWE) under current and future climatic conditions.

Because water resources applications in mountainous areas require model simulations at the watershed or regional scales (Mendoza et al., 2020), spatial discretization strategies are needed to address heterogeneities within the domain of interest. Common choices involve the delineation of grid cells (Liang et al., 1996; Beck et al., 2020), sub-catchments (Bandaragoda et al., 2004) and hydrologic response units (HRUs; Markstrom et al., 2008; Newman et al., 2014) as spatial modeling units. Typically, sub-element variability is also incorporated to improve simulations of the spatial distribution of SWE within each modeling unit (Hartman et al., 1999; Pradhanang et al., 2011; Bajracharya et al., 2018) and to reduce the model sensitivity to changes in the spatial scale (Haddeland et al., 2002). A popular approach is the implementation of subgrid elevation bands, which can account for orographic effects on precipitation and temperature (Abdulla et al., 1996), improving the timing of simulated snowmelt (e.g., Habets et al., 1999; Vicuña et al., 2011) and streamflow dynamics (Abbaspour et al., 2007).

Despite the widespread use of elevation bands in hydrologic and land surface models, there is no guidance for appropriate configuration, based on the effects on simulated hydrological variables (Grusson et al., 2015). Indeed, many studies implementing elevation bands only provide information on the number of snow bands (e.g., Abdulla et al., 1996; Andreadis & Lettenmaier, 2006; Li et al., 2017; Newman et al., 2017; Bajracharya et al., 2018) or the vertical discretization (e.g., Fontaine et al., 2002; Haddeland et al., 2002; Arora et al., 2008), without further details and/or justification of their choice. Improved understanding of effects of elevation bands on simulated states and fluxes is crucial for better characterizations of water resources in mountain domains, given the large effects that subjective modeling decisions may have on hydrological portrayals (Mendoza et al., 2016; Mizukami et al., 2016; Melsen et al., 2019).

To the best of our knowledge, only a few studies have examined the effects of elevation band configurations on hydrologic model simulations. Arola and Lettenmaier (1996) found that adding 10 elevation bands to a lumped model configuration reduced differences in simulated SWE with respect to spatially-aggregated distributed model output in two regions in Montana, USA. Hartman et al. (1999) configured the RHESSys model in the Loch Vale Watershed (Rocky Mountains National Park, Colorado, USA) and compared the effects of adding 200-m and 500-m elevation bands against no bands. In their implementation, they distributed precipitation, air temperature and radiation fluxes at each band, finding (1) little differences among model configurations in catchment-averaged simulated SWE and annual runoff, and (2) that adding elevation bands affected the timing of simulated streamflow. Haddeland et al. (2002) compared model simulations between a 200-m elevation band configuration and no elevation bands, running the Variable Infiltration Capacity (VIC; Liang et al., 1994, 1996) model across different grid resolutions over the Columbia and Arkansas River basins; when no elevation bands were considered, melting occurred earlier, with an increase in evapotranspiration (ET) and, therefore, a shift in both timing and amount of runoff. Essery (2003) compared domain-averaged SWE simulations for the Torne-Kalix River basin (Scandinavia), obtained from a spatially aggregated model, a distributed model with 10 elevation bands, and a 0.25° fully distributed model; they found a close agreement between the latter two configurations - which produced lower peak SWE and extended snow cover duration (compared to the case without bands) -, and found little improvements using four to 10 elevation bands. Clark et al. (2011) showed that disaggregating the

Pinnacle Stream subcatchment (New Zealand) into 100-m elevation bands produced much lower basin-averaged melt rates compared to a spatially lumped configuration. Pradhanang et al. (2011) implemented and calibrated the SWAT model with none, three and five elevation bands (defined with equal areas) in the Cannonsville watershed (New York, USA), distributing daily precipitation and temperature using a simple linear regression with altitude; they found that streamflow simulations were improved when using three elevation bands, with little impacts when further increasing the number of elevation bands.

More recently, Grusson et al. (2015) showed that implementing ten elevation bands in the SWAT model yielded better streamflow simulations, more runoff and less evapotranspiration than two reference simulations (without bands) in the Garonne watershed in France. Bhatta et al. (2019) characterized the effects of geospatial decisions when discretizing the Tamor River basin (eastern Himalayas, Nepal); in particular, they found that moving from one to five elevation bands provided considerable improvements in daily streamflow simulations, and that moving to 10 elevation bands yielded marginal benefits.

None of these studies systematically assessed the effects that the vertical discretization of elevation bands yields on streamflow simulations and annual water balance components, or identified those sub-regions where implementing elevation bands yields large variations in simulated SWE. Hence, this paper addresses the following research questions:

1. How does the configuration of elevation bands affect simulated streamflow, catchment-scale water fluxes and SWE near the date of maximum accumulation?
2. What are the implications of adding elevation bands on simulated SWE at the grid cell scale?
3. What attributes characterize those grid cells where elevation bands make a large difference in simulated SWE?

To seek for answers, we configure the VIC macro-scale hydrological model in nine basins located along the western slopes of the extratropical Chilean Andes. We compare simulation results from a calibrated model without elevation bands (benchmark) with those considering a vertical discretization defined every 1000, 750, 500, 200 and 100 m. We select the VIC model given: (i) the global interest of users (Addor & Melsen, 2019; Sepúlveda et al., 2021) and, therefore, the potential utility of our results for the hydrology community, and (ii) past and ongoing efforts to characterize the current and future hydrology across continental Chile (DGA, 2017; Vicuña et al., 2021; Vásquez et al., 2021). To disentangle the possible role of climatic conditions on inter-model differences, and partially motivated by the negative effects of the ongoing megadrought in Central Chile (Garreaud et al., 2017, 2019), we conduct our assessments for a climatological period (April/1982 – March/2015), a wet period (April/1982 – March/1987) and a dry period (April/2010 – March/2015). A key difference with previous work is that we focus on the sole effects of distributing air temperature with topography, keeping precipitation rates and the rest of meteorological forcings spatially constant across each grid cell.

## 2 Study Domain

We conduct our analyses in nine mountainous basins located along the western slopes of the extra-tropical Andes Cordillera (32.5°-37°S, 70°-71.5°W, Figure 1). These basins were selected based on the following criteria: (i) a near-natural flow regime defined as a maximum

threshold value of 5% for the relationship between annual volume of water assigned as permanent consumptive rights and the mean annual flow (Table 3 in Alvarez-Garreton et al., 2018), (ii) absence of large reservoirs within each catchment, and (iii) small (<2%) glacierized area. Further, these catchments span a wide range of hydroclimatic conditions (Table 1), from high aridity index (2.9) and relatively low mean annual precipitation (486 mm; Estero Pocuro en el Sifón) to low aridity index (0.7) and high mean annual precipitation (1929 mm; Río Ñuble en La Punilla). The southern basins (35°-37°S in Figure 1) also have larger vegetation coverage (just forest fraction coverage shown) due to the lower aridity and increased precipitation, providing higher runoff ratios.

Despite snow being a key component of the water cycle in all case study basins, these encompass different hydrological regimes. This is illustrated in Figure 1 left and right panels), including catchment-scale precipitation and monthly averages of hydrologic variables simulated with the VIC model. Three dominant regimes can be seen: rainfall-driven (Pocuro); snow-dominated (Las Leñas); and mixed regimes where (i) rainfall is the main control for runoff production (Claro), (ii) rainfall and snowmelt contributions are comparable (Ñuble), or (iii) snowmelt dominates catchment-scale hydrology (Arrayán, Mapocho, Colorado, Los Palos and Melado). Interestingly, there are catchments where the seasonal cycles of soil moisture and runoff are similar, regardless of their hydrological regimes (Claro, Las Leñas, Colorado, Palos and Melado), and basins where these cycles are different (Arrayán, Mapocho, Claro and Ñuble).

**Table 1.** List of catchment attributes. Hydrologic variables correspond to the period April/1979 - March/2015. Mean slope and forest fraction were obtained from Alvarez-Garreton et al. (2018).

Catchment	Latitude (°)	Longitude (°)	Area (km <sup>2</sup> )	Mean basin elevation and range (m.a.s.l.)	Mean slope (°)	Mean Annual Precipitation (mm/yr)	Mean Annual AI (PET/P)	Mean Annual Runoff (mm/yr)	Mean Annual Runoff Ratio (-)	Forest fraction (%)
Estero Pocuro en el Sifón	-32.92	-70.54	181	2107 (1002-3695)	22.1	486	2.9	126	0.26	0.2
Estero Arrayán en la Montosa	-33.33	-70.46	216	2469 (969-3833)	24.2	615	2.4	233	0.38	0.4
Río Mapocho en Los Almendros	-33.37	-70.45	638	2936 (970-5428)	25.2	503	2.5	310	0.62	0.4
Río Las Leñas antes junta Río Cachapoal	-34.36	-70.31	172	2865 (1279-4574)	30.4	1266	1.1	752	0.59	0.2
Río Claro en El Valle	-34.69	-70.87	349	1596 (535-3334)	22.2	1422	0.9	862	0.61	27.1
Río Colorado en junta con Palos	-35.28	-71.00	877	2253 (594-4073)	19.6	1802	0.8	1387	0.77	11.5
Río Palos en junta con Colorado	-35.27	-71.02	490	2013 (595-4037)	19.9	1891	0.7	1689	0.89	16.7
Río Melado en el Salto	-35.88	-71.02	2127	2010 (698-3619)	23.5	1766	0.8	1232	0.70	1.9
Río Ñuble en La Punilla	-36.66	-71.32	1254	1711 (566-2617)	23.92	1929	0.7	1718	0.89	13.6

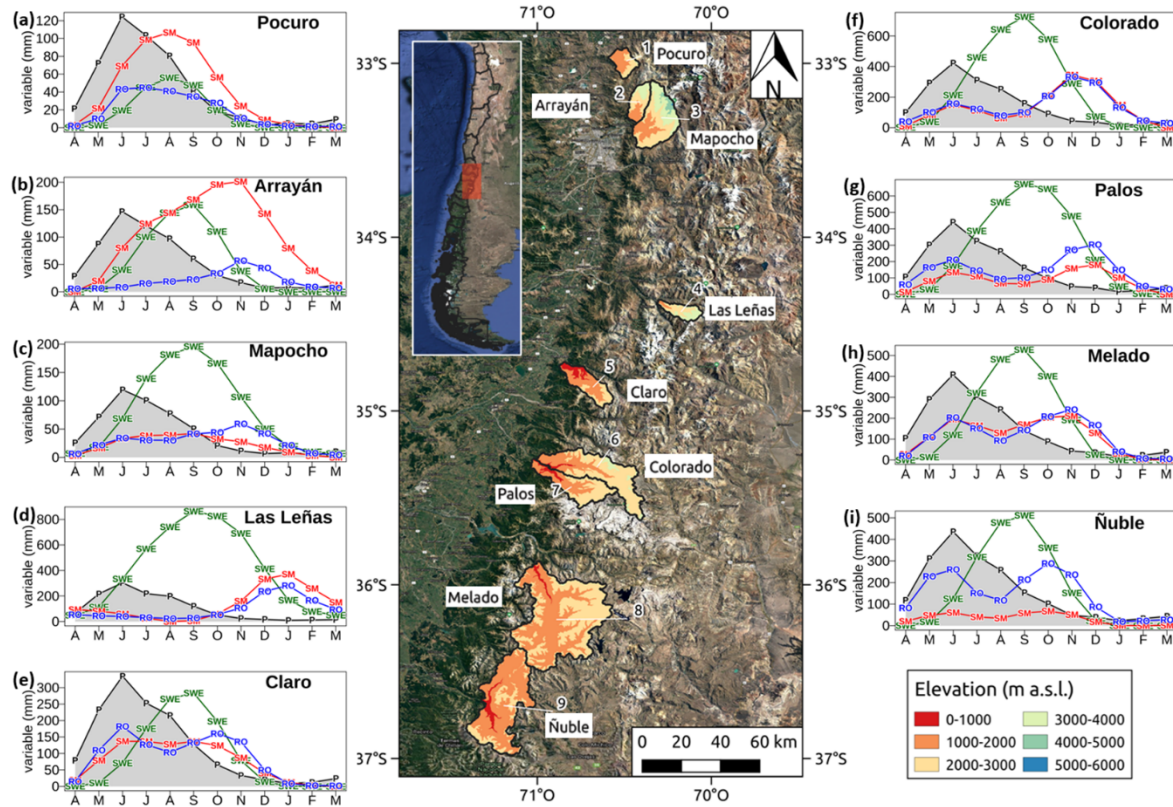


**Figure 1.** Location and elevation of the nine case study basins (center panel), along with seasonal cycles with precipitation (P, black lines and gray areas) and simulated water balance variables (left and right panels) for the climatological period (April/1982-March/2015) - including active soil moisture (SM, red), SWE (green) and runoff (RO, blue) - for the nine case study basins: (a) Estero Pocuro en el Sifón, (b) Estero Arrayán en la Montosa, (c) Río Mapocho en Los Almendros, (d) Río Las Leñas antes junta Río Cachapoal, (e) Río Claro en El Valle, (f) Río Colorado en junta con Palos, (g) Río Palos en junta con Colorado, (h) Río Melado en el Salto, (i) Río Ñuble en La Punilla. For modeled SM, we subtract the lowest mean monthly value of the year so that the plotted values show only the active range of variation.

### 3 Data and Methods

#### 3.1 Meteorological forcings and streamflow data

Daily precipitation and temperature extremes are obtained from an updated version of the CR2MET dataset (Boisier et al., 2018), which has a horizontal resolution of  $0.05^\circ \times 0.05^\circ$ , covering continental Chile for the 1979-2016 period. The dataset for precipitation was generated with a statistical post-processing technique that uses topographic descriptors and large-scale climatic variables (water vapor and moisture fluxes) from ERA-Interim (Dee et al., 2011) and ERA5 (C3S & Copernicus Climate Change Service (C3S), 2017) as predictors, and observed daily precipitation from gauge stations as predictand. For the case of maximum and minimum daily temperature, additional variables from MODIS land surface products were added as predictors. Daily precipitation and temperature time series are disaggregated into 3-hourly time steps using the sub-daily distribution provided by ERA-Interim. Relative humidity and wind speed are derived for the

same horizontal resolution grid by spatially interpolating a blend between ERA-Interim and ERA5 datasets, because the latter was not available for the entire study period (1985–2015) at the moment of data acquisition (early 2018). Despite the short temporal coverage from ERA5 (2010–2016), the updated reanalysis information was included for a better spatial representation of the mega drought (Garreaud et al., 2019; Vicuña et al., 2021).

Streamflow data is obtained from stations maintained by the Chilean Water Directorate (DGA, available from the CR<sup>2</sup> Climate Explorer <https://www.cr2.cl/datos-de-caudales/>).

### 3.2 Hydrological model

We use the Variable Infiltration Capacity (VIC; Liang et al., 1994, 1996) model, which is a macro-scale, process-based and semi-distributed hydrologic model. In VIC, the modeling unit is the grid cell, which is defined here to match the meteorological forcing data resolution (i.e.,  $0.05^\circ \times 0.05^\circ$ ). The model is run at 3-hourly time steps. Interception is simulated with a one-layer canopy reservoir that is emptied by canopy evaporation, transpiration, or throughfall, which occurs when additional precipitation exceeds the storage capacity of the canopy. Different vegetation classes are allowed in each grid cell through a mosaic approach, where water and energy balance terms are computed independently for each coverage class (vegetation and bare soil). Each grid cell has three soil layers: the two upper layers represent the interaction between soil moisture and vegetation, while the bottom layer simulates baseflow processes. It should be noted that VIC does not consider lateral exchange of fluxes between grid cells, which implies that water can only enter a grid cell from the atmosphere. A two-layer energy balance model is used to simulate snowpack dynamics: the upper layer solves the energy balance between the atmosphere and the snowpack, and the bottom layer stores the excess snow mass from the upper layer (Cherkauer & Lettenmaier, 2003; Andreadis et al., 2009).

### 3.3 Experimental setup

#### 3.3.1 Benchmark model

To assess the effects of including elevation bands on simulated states and fluxes, we compare VIC simulations with different elevation band implementations against a benchmark model based on the work by Vásquez et al. (2021). In such implementation, a priori distributions for vegetation parameters were obtained using the land cover classes described in Zhao et al. (2016); spatial information on hydraulic conductivity values was obtained from the Natural Resources Data Center (CIREN for its acronym in Spanish) and all grid cells were considered flat (i.e., no elevation bands are defined). In our setup, all model simulations are conducted in full energy balance mode – dismissing frozen soil processes –, and no horizontal runoff routing is performed since, for the contributing catchment areas examined here, routing effects are not expected to be important at the daily or longer time scales (Gericke & Smithers, 2014; Beck et al., 2020). Therefore, modeled streamflow is obtained from basin-averaged runoff.

The parameters for the benchmark model (Table 2) are calibrated using the Shuffled Complex Evolution global optimization algorithm (SCE; Duan et al., 1993). All soil parameters are considered spatially constant within each catchment (i.e., no parameter regularization was considered). The objective function is the Kling-Gupta Efficiency metric (Gupta et al., 2009):

$$KGE = 1 - \sqrt{(r - 1)^2 + (\alpha - 1)^2 + (\beta - 1)^2} \quad (1)$$

where  $r$  is the Pearson correlation coefficient between simulated and observed runoff;  $\alpha$  is the ratio of the standard deviation of simulated values to the standard deviation of observed values; and  $\beta$  is the ratio between the mean of the simulated values to the mean of observations.

The calibration process considers streamflow data for at least four years within the period April/1990-March/2010, and if the minimum record length is not satisfied, the periods April/1985-March/1990 and April/2010-March/2015 are considered. All model simulations are conducted for the period Jan/1979-Dec/2015, using the first three years to initialize model states. If two or more parameter sets yield the same KGE values, we select the one that maximizes the Nash-Sutcliffe efficiency (NSE; Nash & Sutcliffe, 1970). The parameter sets found in this step are used for subsequent modeling experiments (section 3.3.2) - i.e., no parameter recalibration is performed.

**Table 2.** List of VIC parameters and limits considered for calibration.

Parameter	Description	Units	Calibration range	
			Min	Max
infiltr	Variable infiltration curve parameter ( $b_{infiltr}$ )	-	0.001	0.162
$D_s$	Fraction of $D_{smax}$ where non-linear baseflow begins	-	0.312	0.806
$D_{smax}$	Maximum velocity of baseflow	mm/day	83.2	183.2
$W_s$	Fraction of maximum soil moisture where non-linear baseflow occurs	-	0.108	0.900
C	Exponent used in baseflow curve	-	3.0	10.9
depth <sub>1</sub>	Thickness of each soil moisture layer	m	0.014	2.169
depth <sub>2</sub>		m	0.418	5.281
depth <sub>3</sub>		m	0.173	3.753
$K_{sat}$	Saturated hydraulic conductivity	mm/day	1499	2565
Newalb	Fresh snow albedo		0.725	0.950
$Alb_{acum\ a}$	Snow albedo curve parameter	-	0.725	0.950
$Alb_{thaw\ a}$	Snow albedo curve parameter	-	0.883	0.920
$T_{rain}$	Minimum temperature for rainfall occurrence	°C	-2.735	3.446
$r_{snow}$	Snow surface roughness	m	1.24E-5	0.022

### 3.3.2 Alternative model configurations

Figure 2 illustrates how elevation bands can be configured in VIC. It can be noted that the model lumps all areas within the same elevation range into one band. Additionally, fluxes and state variables for each band are weighted by area fraction to provide grid-cell averages.



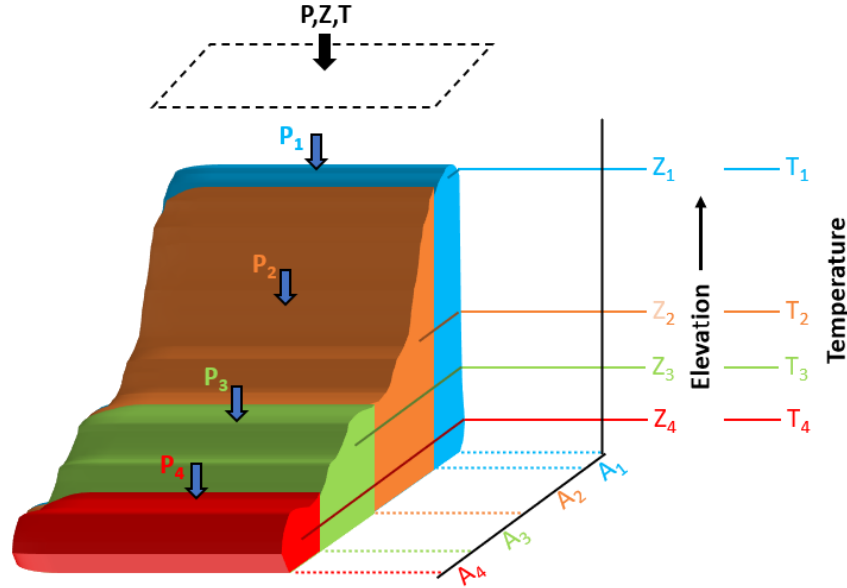


**Figure 2.** Spatial representation of subgrid elevation bands in VIC. A, P, T, and Z denote area, average precipitation, air temperature, and terrain elevation for each elevation band.

For each basin, we create five alternative model configurations by spatially disaggregating all grid cells into 1000 m, 750 m, 500 m, 200 m and 100 m elevation bands, using the Advanced Spaceborne Thermal Emission and Reflection (ASTER) global Digital Elevation Model (reference). To harmonize all these spatial configurations, we consider 0 m a.s.l. as the starting point of elevation bands for all catchments, instead of the lowest point of each catchment's grid cell. For the lowest and the highest elevation bands, we set a minimum fractional area of 5% (with respect to the grid cell's area); if such a condition is not met, that band (i.e., the lowest and/or the highest) is merged to the closest one. This implies that peak elevations may be excluded from our representation of subgrid variability.

In all alternative model configurations, precipitation rates are assumed to be constant with elevation, but air temperature is lapsed from the mean grid cell elevation to each elevation band using local lapse rates. To this end, we cluster our basins into three groups (basins 1-3, 4-7 and 8-9 in Figure 1) based on spatial proximity, and compute lapse rates using the mean annual temperatures obtained from the grid cells belonging to each cluster. It should be noted that these lapse rates are not affected by the configuration of elevation bands, since they are computed from a meteorological product (CR2MET) that assumes flat grid cells. All simulations with elevation bands are performed in full energy balance mode, without horizontal runoff routing.

### 3.3.3 Analysis framework

We select three continuous periods for analysis based on observed catchment-scale precipitation and runoff: (i) a 5-year wet period, (ii) a 5-year dry period, and (iii) a climatological period that spans April/1982 – March/2015, including (i) and (ii). The choice of wet and dry periods is based upon visual inspection of annual precipitation time series and the calculation of 5-year moving averages of precipitation and runoff. The wet period (April/1982 – March/1987) begins after a long epoch with a persistent negative trend in annual precipitation across semi-arid central Chile (30-35°S) from the beginning of the 20<sup>th</sup> century until the mid-1970s (Quintana &

Aceituno, 2012). The dry period (April/2010 – March/2015) covers the first half of the megadrought, when severe annual rainfall deficits (25-45%) prevailed in central Chile (30-38°S), diminishing the Andean snowpack and resulting in amplified declines of river flow (up to 90%), reservoir volumes and groundwater levels (Garreaud et al., 2017).

First, we assess the capability of the benchmark model and each alternative model configuration (i.e., six model configurations in total) to reproduce observed daily runoff, flow duration curves and runoff seasonality. In this analysis, flow duration curves and runoff seasonality graphs are calculated for the climatological period. We compute the KGE and NSE for modeled runoff at daily and monthly time steps. Additionally, we examine the percent bias for the midsegment slope (%BiasFMS) and the low-segment volume (%BiasFLV) of the flow duration curves (Yilmaz et al., 2008):

$$\%BiasFMS = \frac{[\log(QS_{m1}) - \log(QS_{m2})] - [\log(QO_{m1}) - \log(QO_{m2})]}{[\log(QO_{m1}) - \log(QO_{m2})]} \cdot 100 \quad (2)$$

$$\%BiasFLV = -1 \cdot \frac{\sum_{l=1}^L [\log(QS_l) - \log(QS_L)] - \sum_{l=1}^L [\log(QO_l) - \log(QO_L)]}{\sum_{l=1}^L [\log(QO_l) - \log(QO_L)]} \cdot 100 \quad (3)$$

where QS is the simulated flow [m<sup>3</sup>/s], QO is the observed flow [m<sup>3</sup>/s], m1 and m2 are the lowest and highest flow exceedance probabilities (0.2 and 0.7, respectively), and L is the index of the minimum flow.

Then, we compute percent changes between alternative model configurations and the benchmark model results to quantify the effects of adding elevation bands on simulated input/output fluxes and SWE. Specifically, we examine mean annual rainfall, snowfall, runoff, sublimation, snowmelt and ET, as well as September 1 SWE (SWE 09/01 hereafter) – which is used to produce operational seasonal streamflow forecasts in central Chile (Mendoza et al., 2014) –, at both catchment and grid cell (i.e., 0.05°) scales.

To analyze in detail the effects of snow bands with different vertical discretizations on simulated daily SWE, albedo, cumulative sublimation and cumulative snowmelt, we select three grid cells with different locations, mean elevations, and elevation ranges within the Mapocho River basin (Figure 3). These comparisons are conducted for water years selected from our wet and dry periods to examine the interplay between hydroclimatic conditions and the configuration of elevations bands.

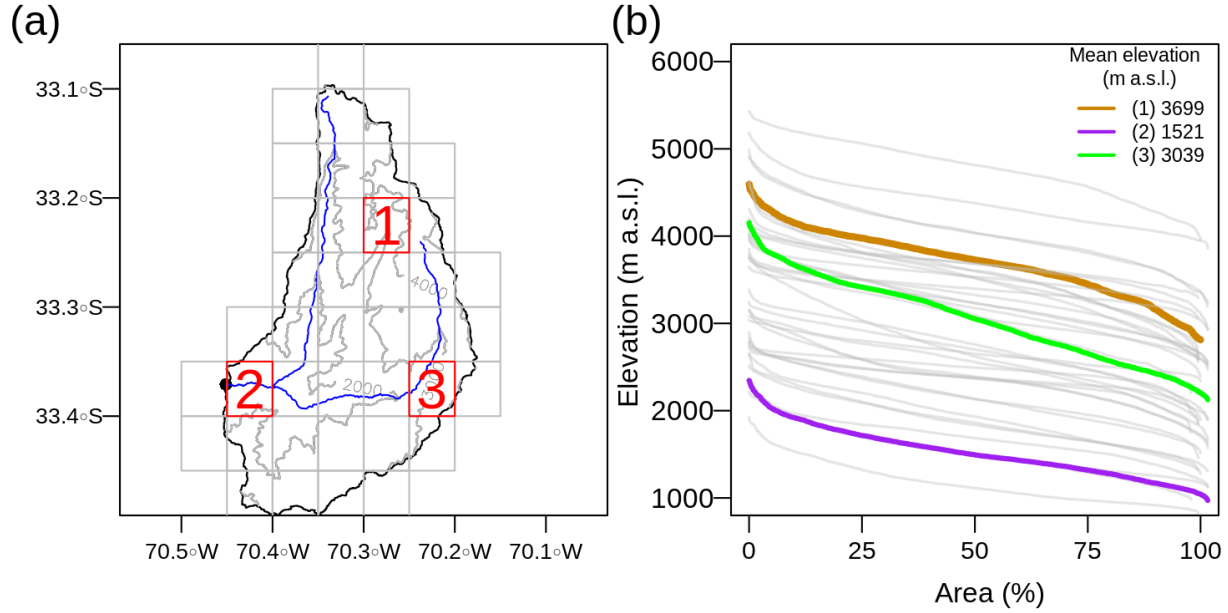


**Figure 3.** (a) Selected grid cells of the Mapocho River basin; the black dot represents the catchment outlet. (b) Hypsometric curves of the grid cells displayed in panel (a), including those selected for detailed analysis.

To identify the most sensitive grid cells and model configurations in terms of snow accumulation, we compare SWE 09/01 (i.e., SWE at the beginning of snowmelt season) obtained from the 200-m configuration and the benchmark, for all water years (i.e., 33) in the climatological period. We define a grid cell as sensitive if differences in simulated SWE 09/01 with respect to the benchmark model are larger than 10% for >50% of water years. To seek for controls on different grid cell behavior, we compare the cumulative distribution functions (CDFs) of several attributes (Table 3) obtained from sensitive vs. insensitive grid cells. We also contrast CDFs of state variables and fluxes simulated with the 200-m model configuration in sensitive vs. insensitive grid cells, including rainfall, snowfall, ET, runoff, snowmelt, and maximum SWE. In all these comparisons, we perform Kolmogorov-Smirnov tests and report associated p-values.

**Table 3:** Attributes considered for each grid cell. Calculations consider water years (April-March).

Attributes name	Description	Units	Formula
Altitude	Mean elevation	m a.s.l.	-
Range	Difference between maximum and minimum altitude.	m	$Z_{\max} - Z_{\min}$
Aspect	Average grid cell aspect, calculated counterclockwise from east.	°	-
Slope	Mean slope across each grid cell	°	-
Annual temperature (T)	Annual T for a specific water year	°C	$\frac{1}{N} \sum_{i=1}^N T_{daily}$
Annual precipitation (P)	Annual P for a specific water year	mm/yr	$\sum_{i=1}^N P_{daily}$

Attributes name	Description	Units	Formula
Annual Moisture Index ( $I_m$ ) <sup>1</sup>	Indicates whether climatic conditions are arid (water-limited) or humid (energy-limited). Ranges from -1 to 1, with negative and positive values for arid and humid conditions, respectively.	-	$I_m = \frac{1}{12} \sum_{t=1}^{t=12} MI(t)$ <p>Where:</p> $MI(t) = \begin{cases} 1 - \frac{E_p(t)}{P(t)}, & P(t) > E_p(t) \\ 0, & P(t) = E_p(t) \\ \frac{P(t)}{E_p(t)} - 1, & P(t) < E_p(t) \end{cases}$
Moisture Index Seasonality ( $I_{mr}$ ) <sup>1</sup>	Indicates intra-annual changes in the water/energy budget. Ranges from 0 (no variability) to 2 (very large variability)	-	$I_{m,r} = (MI(1,2, \dots, 12)) - (MI(1,2, \dots, 12))$
Fraction of annual precipitation that occurs as snowfall ( $f_s$ ) <sup>1</sup>	Ranges from 0 to 1, where 0 indicates no snowfall in a year and 1 that all precipitation occurs as snow.	-	$f_s = \frac{\sum \text{monthly snowfall}}{\sum \text{monthly precipitation}}$

N is the number of days in each water year.

## 4 Results

### 4.1 Model evaluation against observed streamflow

Figure 4 compares modeled daily runoff time series against observations for water year (WY) 2009/2010 (as an example), as well as mean monthly runoff and daily flow duration curves for the climatological period. The results show small differences between the benchmark model (i.e., no elevation bands) and the alternative model configurations. Adding elevation bands provides a maximum KGE increment of 0.03 for daily streamflow throughout all basins during WY 2009/2010 (see Table 4). All model configurations underestimate daily peak flows during winter (e.g., f.1 and h.1) and fail to capture streamflow recessions, providing slower (e.g., see panel f.1 between June and August) or faster (e.g., see panel i.1 between July and August) responses compared to observed runoff. In the Palos River basin (Figure 4g.1), there are notable discrepancies in December arising from different vertical discretizations. Figure 4 also shows that all model configurations capture catchment-scale runoff seasonality reasonably well, excepting Estero Arrayán (Figure 4b.2), where rainfall contributions to runoff are underestimated, or the Las Leñas basin (Figure 4d.2), where modeled maximum monthly values are delayed. In some cases, observed monthly values are overestimated (e.g., Pocuro basin, Figure 4a.2) or underestimated (e.g., December to March at the Ñuble basin, Figure 4i.2; near August, Figure 4g.2).

**Table 4:** KGE values for simulated daily runoff - WY 2009/2010.

Model configuration	Pocuro	Arrayán	Mapocho	Las Leñas	Claro	Colorado	Palos	Melado	Ñuble
---------------------	--------	---------	---------	-----------	-------	----------	-------	--------	-------

<sup>1</sup> These climate indices were used in Knoben et al. (2018). It should be noted that the fraction of annual precipitation that occurs as snow ( $f_s$ ) was not calculated as in Knoben et al. (2018), because VIC computes snowfall considering a minimum temperature at which rainfall can occur and a maximum temperature at which snowfall can occur, rather than using a single temperature as threshold.

No Bands (NB)	0.73	0.58	0.58	0.79	0.51	0.64	0.70	0.69	0.32
1000 m	0.74	0.58	0.59	0.81	0.51	0.65	0.70	0.69	0.33
750 m	0.74	0.58	0.59	0.79	0.51	0.65	0.70	0.69	0.33
500 m	0.74	0.58	0.61	0.80	0.51	0.65	0.73	0.69	0.34
200 m	0.74	0.59	0.60	0.81	0.51	0.65	0.72	0.68	0.34
100 m	0.74	0.58	0.60	0.81	0.51	0.65	0.72	0.68	0.34

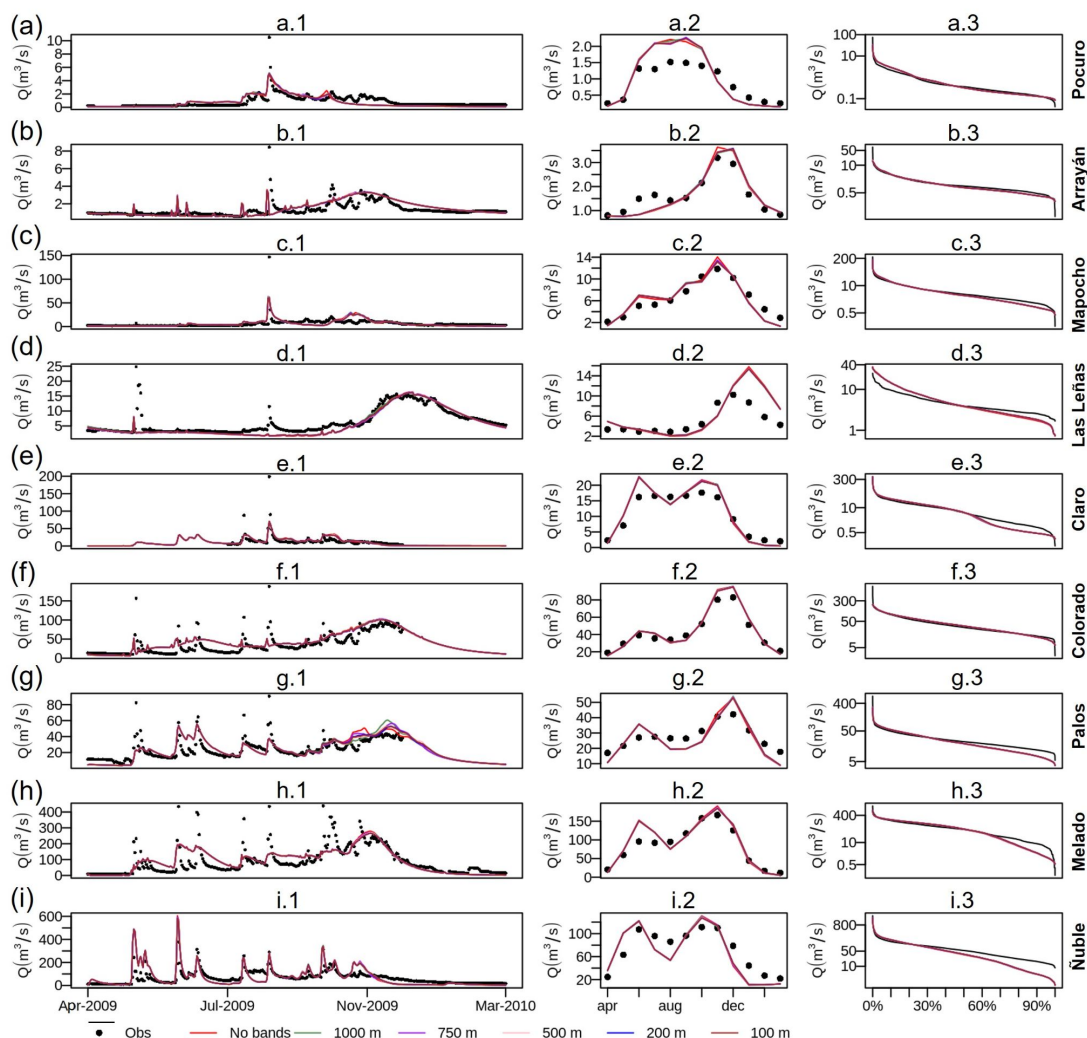
The results for the percent bias in the mid-segment slope of the flow duration curves (%BiasFMS, Table 5) show that all model simulations yield flashier responses compared to observed runoff in all basins. When adding elevation bands, %BiasFMS increases in the Pocuro and Arrayán basins compared to the benchmark model, with maximum variations of 2.1% and 3.7% using the 100-m configuration, respectively, and these changes do not necessarily correlate with increased vertical resolution. However, elevation bands provide improvements (i.e., decrease in %BiasFMS) in the rest of the basins, ranging from 0.3% for the Claro River basin (200-m configuration) to 8.3% for Las Leñas River basin (200-m configuration).

The incorporation of elevation bands yields reductions in the percent bias in FDC low-segment volume (%BiasFLV, Table 5) in all catchments excepting the Mapocho River basin. As with %BiasFMS, improvements in %BiasFLV are not correlated with the vertical resolution, and they range from 0.01% for Pocuro (1000-m configuration) to 1.03% for Las Leñas (200-m configuration). However, large negative biases in simulated long-term baseflow responses are obtained in some basins (Figure 4, panels c.3, d.3, e.3, g.3, h.3 and i.3) with all model configurations.

**Table 5:** Model evaluation metrics derived from the daily flow duration curve (April/1982-March/2015).

Metric	Config.	Pocuro	Arrayán	Mapocho	Las Leñas	Claro	Colorado	Palos	Melado	Ñuble
%BiasFMS	No Bands (NB)	15.5	21.6	22.6	53.4	45.8	5.2	52.9	31.2	59.9
	1000 m	17.6	25.3	22.1	47.3	46.0	4.7	50.1	27.8	57.7
	750 m	16.0	23.2	20.8	46.5	46.1	4.8	50.8	27.4	57.3
	500 m	16.7	23.2	22.3	45.8	45.4	4.7	49.3	25.9	55.8
	200 m	16.9	24.1	22.4	45.1	45.5	4.4	48.4	24.9	56.0
	100 m	17.4	23.9	22.2	45.2	45.4	4.5	47.8	24.8	55.6
%BiasFLV	No Bands (NB)	2.0	5.4	6.9	6.5	14.4	0.8	6.3	14.2	16.1
	1000 m	2.0	5.3	7.2	5.7	14.3	0.8	6.2	13.6	15.9
	750 m	1.9	5.2	6.9	5.6	14.3	0.8	6.2	13.6	15.9
	500 m	2.0	5.2	7.1	5.5	14.2	0.7	6.1	13.4	15.8
	200 m	2.0	5.1	7.0	5.5	14.2	0.7	6.0	13.2	15.7
	100 m	2.0	5.1	7.1	5.5	14.2	0.7	6.0	13.1	15.7

365



366

367 **Figure 4.** Comparison between simulated and observed runoff ( $Q$ ) for all basins in terms of daily  
 368 time series (April/2009-March/2010, left panels), mean monthly runoff (center panels) and daily  
 369 flow duration curves (right panels, vertical logarithmic scale). The results in center and right panels  
 370 correspond to the climatological period. In the left panels, missing dots indicate the absence of  
 371 runoff measurements.

372 Figure 5 illustrates the sensitivity of KGE to the configuration of elevation bands across  
 373 basins and analysis periods, for daily (top panels) and monthly (bottom panels) runoff. In general,  
 374 these results reinforce the idea that adding elevation bands has marginal effects on simulated basin-  
 375 averaged runoff, yielding KGE improvements ( $\Delta KGE$ ) during the 5-year wet period that range  
 376 from 0 to 0.05 (Palos basin) for both daily (Figure 5a) and monthly (Figure 5d) time scales. During  
 377 the 5-year dry period (Figures 5b and 5e), the overall KGE improvement (average from all  
 378 catchments) is 0.02, with the largest increments obtained for the Palos and Mapocho River basins  
 379 (although the resulting KGE is still low), and negligible variations ( $\sim 0.01$ ) in the remaining basins.

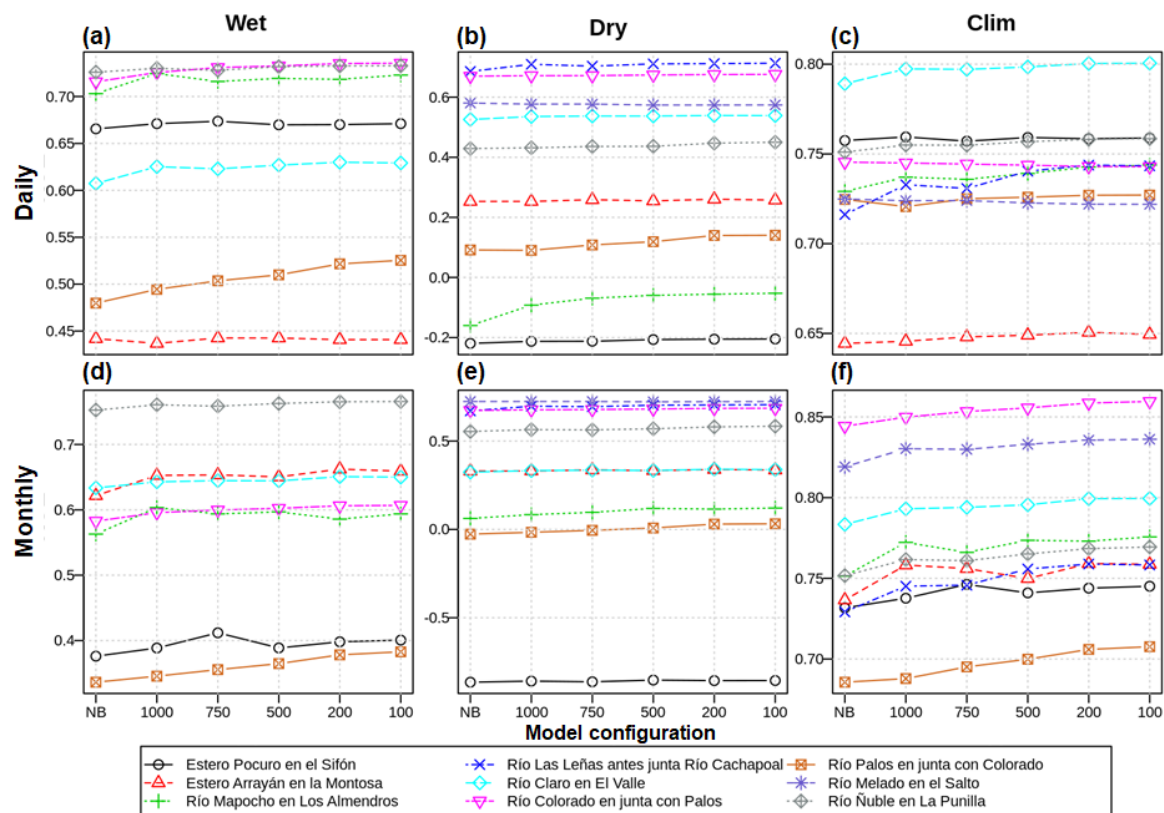


**Figure 5.** KGE results computed with daily (top) and monthly (bottom) runoff, obtained from the benchmark (NB: No Bands) and the five alternative model configurations (i.e., using 1000-m, 750-m, 500-m, 200-m, and 100-m elevation bands). Each curve displays individual basin results, and missing basins in some panels indicate the absence of verification (i.e., observed) data for that period.

During the climatological period (Figures 5c and 5f), similar performance metrics are obtained for the 200-m and 100-m configurations. For daily runoff simulations (Figure 5c), adding elevation bands provides KGE improvements ranging 0.02-0.03 in Las Leñas and Mapocho basins, and slight KGE reductions (less than 0.01) in the Colorado and Melado basins. KGE values obtained from monthly runoff simulations (Figure 5f) increase between 0.01 and 0.03 in all basins when 200-m and 100-m configurations are used.

The results displayed in Figure 5 show that incorporating elevation bands generally yields slight improvements in streamflow simulations in terms of KGE; however, a higher vertical resolution does not necessarily translate into increased KGE in all basins (e.g. see results for Estero Arrayán in Figures 5a, 5b and 5c). A noteworthy result from Figure 5 is the constant, larger positive effect on KGE that adding elevation bands provides in the Palos River basin during the wet period compared to the dry period, which may be explained by the linear shape of its hypsometric curve over most of its fractional area (not shown), favoring more evenly distributed areas across elevation bands. More generally, Figure 5 shows that the effects of increased vertical resolution are not necessarily linear, i.e., some ‘coarse’ model configurations provide better KGE results than configurations with more elevation bands, yet both configurations are an improvement compared to the benchmark (see, for example, 750-m configuration results for the Pocuro basin in Figure 5d,

and 1000-m configuration results of the Arrayán basin in Figure 5f). The analysis of KGE components (see Figures for Supplement S4, S5 and S6) reveals a similar behavior for these metrics, i.e., slight variations of results with the choice of snow band configuration during the dry period, and changes in both wet and climatological periods. The largest impacts of alternative model configurations are obtained for the  $\alpha$  component (Figure S5), with a moderate reduction.

The effects of adding elevation bands are somewhat different for NSE, for which improvements during the wet and climatological periods are greater than the response of KGE, especially in the Arrayán River basin. Further, negligible changes in NSE are observed during the dry period (Figure S3).

#### 4.2 Effects on mean annual fluxes and September 1<sup>st</sup> SWE

Figure 6 illustrates the effects of adding elevation bands on simulated basin-averaged mean annual fluxes and SWE 09/01. Overall, changes in annual averages are smaller than 5% (with a few exceptions). Differences between alternative configurations are usually smaller than differences between the benchmark and any model configuration with elevation bands, and the effects of increasing the vertical resolution are very small beyond 200-m. Further, variations produced by alternative model configurations are not necessarily proportional to the vertical resolution of elevation bands, and the sign of such impacts in a specific catchment may differ depending on the analysis period.

The alternative model configurations produce slight variations in mean annual runoff, with ~0.15% reductions during the wet and climatological periods in most basins. During the dry period, small reductions (<0.1%) are obtained in the Colorado, Melado and Ñuble River basins. The Arrayán River basin is the only catchment where the inclusion of elevation bands slightly increases (~0.5%) the mean annual runoff in all analyses. These small variations in mean annual runoff – compared to the other variables displayed in Figure 6 – suggest that the similarity in KGE values obtained for daily and monthly runoff with all model configurations (Figure 5) may be attributed to very different reasons. Indeed, mean annual rainfall decreases in seven catchments (i.e., all basins except Las Leñas and Mapocho) around 0.7-0.9% during the wet period, as the number of elevation bands increases due to changing the snow-rain partitioning of precipitation. Very similar variations are observed during the dry and climatological periods; even more, the inclusion of more elevation bands also yields less rainfall during the dry period in the Mapocho River basin. Conversely, average increases of 2-3% in mean annual snowfall are obtained with the alternative model configurations.

The implementation of elevation bands results in mixed variations across catchments in basin-averaged SWE 09/01 with respect to the benchmark model. Negative changes are obtained in Las Leñas and Colorado River basins during all analysis periods; and small (<0.5%) negative variations in SWE 09/01 are obtained in the Palos River basin during the dry period. In the remaining basins, more SWE 09/01 is simulated with the alternative model configurations, and variations depend on the analysis period and vertical discretization.

Interestingly, the results in Figure 6 show that more simulated snowfall does not necessarily yield more SWE 09/01. For example, adding elevation bands increases snowfall in the Colorado River basin in all analysis periods, producing less SWE 09/01 compared to the benchmark model. Additionally, all alternative configurations provide more snowfall in the Pocuro



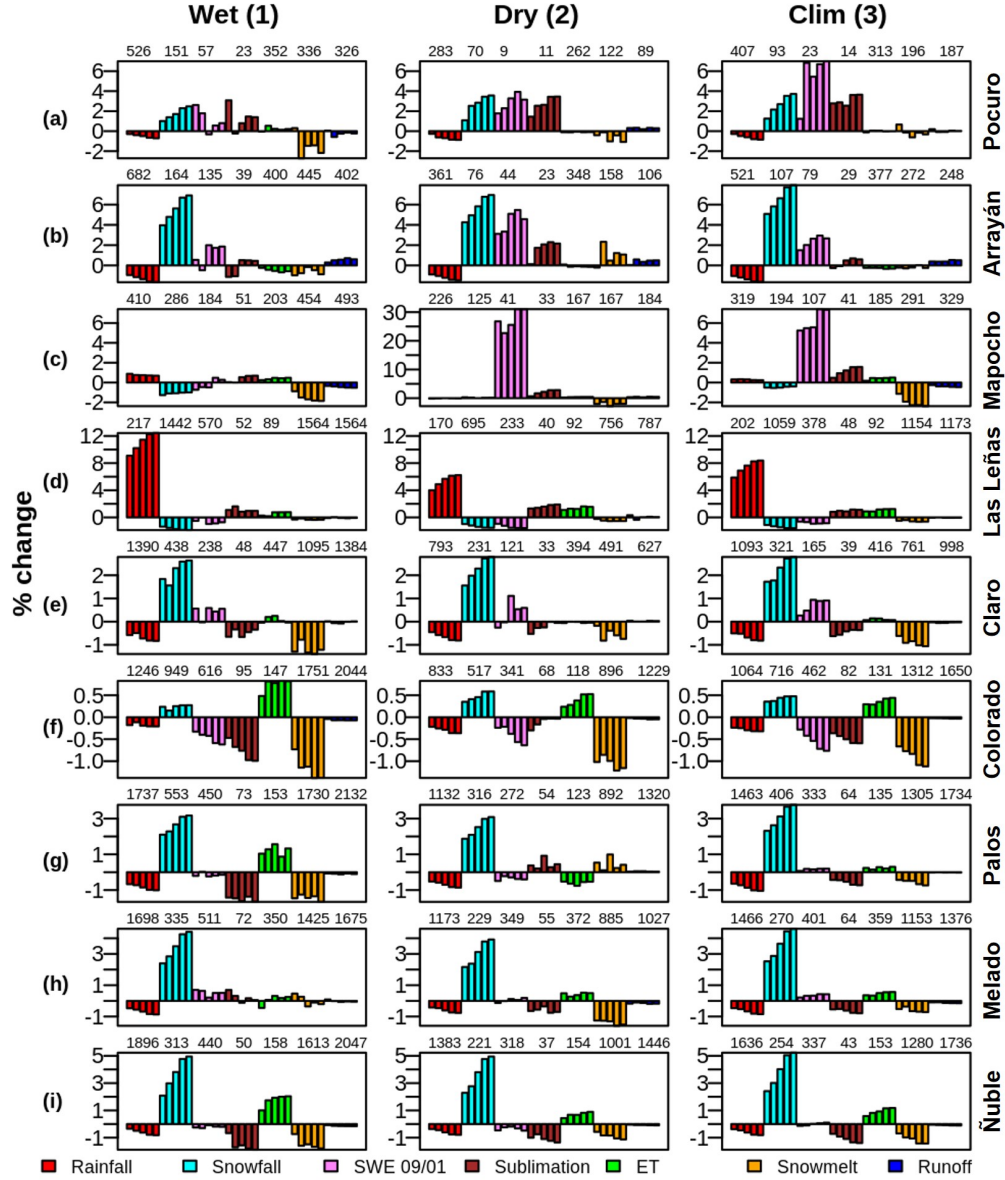
River basin; however more SWE 09/01 is obtained during the dry period and the climatological period, and less SWE 09/01 during the wet period.

Figure 6 also shows that incorporating subgrid elevation bands generally yields less snowmelt with a few exceptions (i.e., Figures 5a.3, 5b.2, 5g.2, 5h.2), and mixed variations in annual sublimation amounts. Indeed, elevation bands tend to provide more sublimation in northern, water limited (i.e.,  $PET/P > 1$ ) catchments (e.g., Figures 5a to 5d), and generally less sublimation in energy limited (i.e.,  $PET/P < 1$ ) basins. Additionally, part of the rainfall feeds the snowpack, providing liquid water that contributes to increase SWE during the winter season, which explains why VIC produces more annual snowmelt than annual snowfall. For example, the mean annual snowfall obtained with the baseline model at the Pocuro River basin is 93 mm/yr, while the mean annual snowmelt for the same period is 196 mm/yr.

Slight increases ( $\sim 0.6\%$ ) in simulated basin-averaged ET are obtained with the alternative model configurations during the wet (except Arrayán, with  $\sim 0.5\%$  decreases) and climatological periods. During the dry period, the addition of elevation bands yields less simulated ET in four basins (Pocuro, Arrayán, Claro and Palos).

We now examine intra-catchment variability in changes induced by the alternative model configurations on simulated hydrological variables. Specifically, we assess percent changes  $[100 \cdot (\text{alternative} - \text{benchmark}) / \text{benchmark}]$  in simulated mean annual fluxes and SWE 09/01 at each grid cell across the Mapocho River basin (Figure 7). The same figures for the remaining catchments are included in the supplementary information (S7-S14). It can be noted that the effects of elevation bands on mean annual rainfall are more evident in high elevation areas (over 3,000 m a.s.l.), where larger increments (all computed as the mean from the alternative configurations) are obtained during the wet period ( $\sim 9\%$  average; Figure 7a) compared to the dry period ( $\sim 2\%$  average; Figure 7b); additionally, rainfall increments are larger than 20% in some high-elevation grid cells during the wet period. Conversely, the incorporation of elevation bands yields less rainfall in low elevation grid cells, with declines  $< 5\%$ .

As expected, simulated snowfall increases in grid cells located below 2,500 m a.s.l. when elevation bands are included, with larger increments for higher vertical resolutions. Snowfall variations in low-elevation areas are larger during the wet period using all alternative model configurations, spanning +20-50%. Further, adding elevation bands in the Mapocho River basin decreases snowfall amounts less than 10% in some grid cells located above 2,500 m a.s.l. The largest variations in SWE 09/01 generally occur below 3,000 m a.s.l., and these are more pronounced during the dry period; however, this behavior is not observed in the rest of the basins (see from Supplementary Figure S7 - Figure S14). Simulated annual sublimation and snowmelt can be largely affected by the inclusion of elevation bands. Interestingly, the sign and magnitude of snowmelt variations does not necessarily match the spatial patterns of changes in SWE 09/01. Finally, Figure 7 shows that the alternative model configurations do not induce substantial changes in mean annual ET and runoff across the basin of interest, which is also observed in the remaining basins.



**Figure 6.** Percent changes  $[100 \cdot (\text{alternative} - \text{benchmark}) / \text{benchmark}]$  in simulated basin-averaged mean annual fluxes and SWE 09/01 for different periods (columns) and all case study basins. In each panel, the bars holding the same color represent, from left to right, percent changes for model configurations with 1000 m, 750 m, 500 m, 200 m and 100 m elevation bands. The numbers placed over each set of bars indicate the values obtained with the benchmark model (in mm/year for fluxes and mm for SWE 09/01). Note that a different axis range is used for the Mapocho River basin during the dry period (b), due to overaccumulation on a grid cell with glacierized area (not shown here) which affects simulated SWE 09/01.

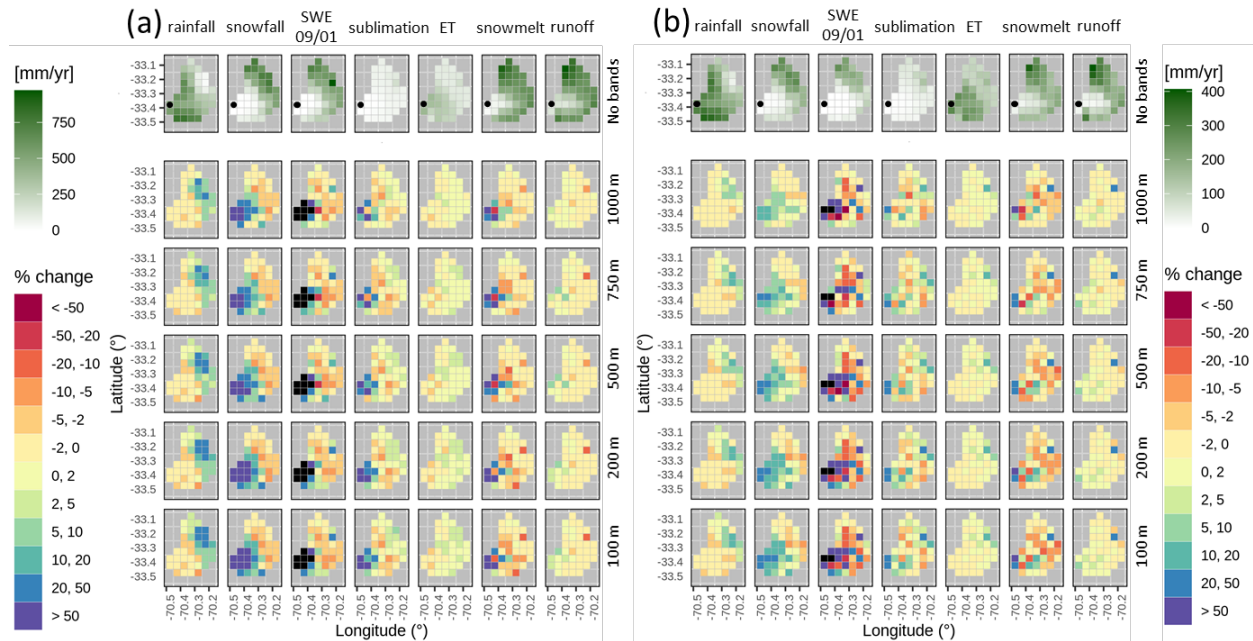


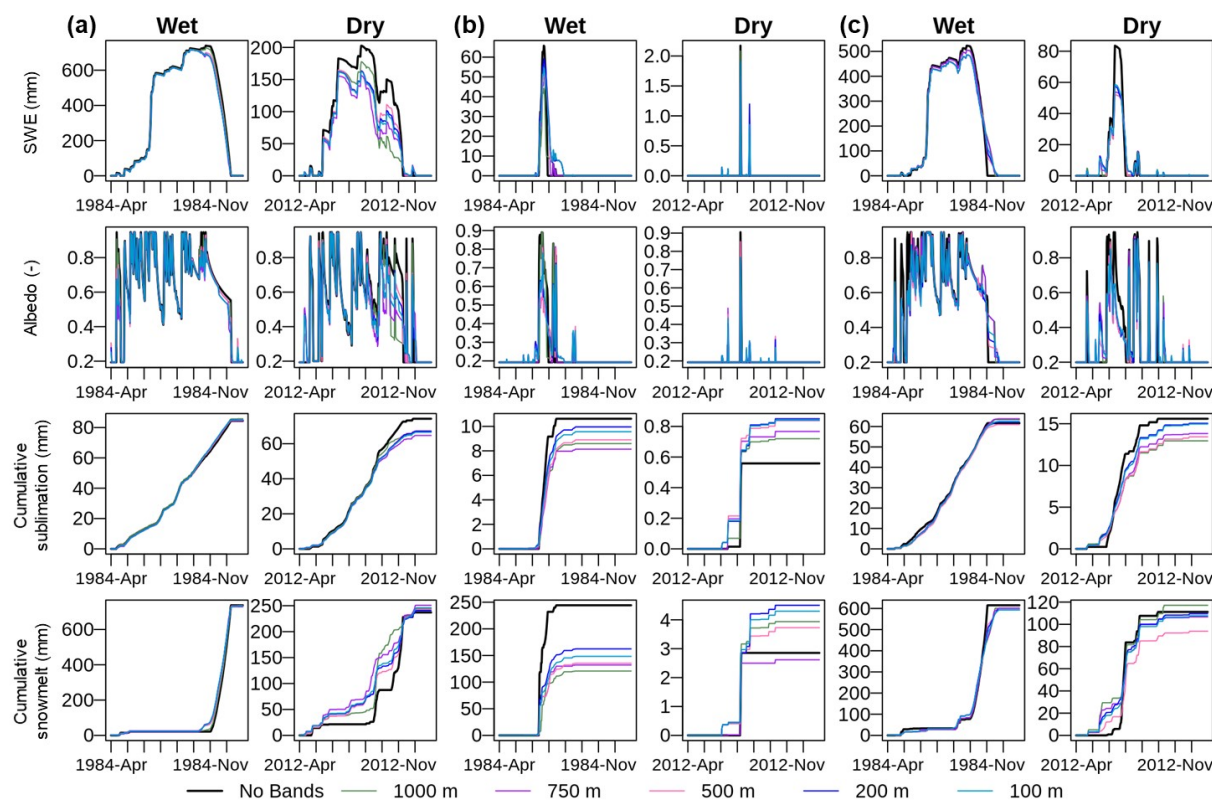
**Figure 7.** Spatial variability of percent changes  $[100 \times (\text{alternative} - \text{benchmark}) / \text{benchmark}]$  in grid cell-scale simulated mean annual fluxes and SWE 09/01 at the Mapocho River basin. Results are presented for (a) wet and (b) dry analysis periods. The various columns display, from left to right, results for mean annual rainfall, mean annual snowfall, mean SWE 09/01, mean annual sublimation, mean annual ET, mean annual snowmelt and mean annual runoff. The top row displays results for the benchmark model in mm/yr (excepting SWE 09/01, presented in mm), while the remaining rows show results for alternative model configurations (i.e., 1000, 750, 500, 200 and 100 m elevation bands, from top to bottom). Black tiles indicate no data, associated with benchmark model results equal to zero (or unbounded result). The black dot in the top row represents the catchment outlet.

#### 4.3 Differences in simulated daily SWE

We examine simulations of daily SWE and three related variables (albedo, cumulative sublimation and cumulative snowmelt) in three grid cells of the Mapocho River basin (Figure 3) during WYs 1984 and 2012, characterized by wet and dry conditions, respectively (Figure 8). Model simulations with elevation bands yield less SWE in all grid cells during WY 1984 (wet), and snow disappearance gets delayed in grid cells (2) and (3) compared to the benchmark model. In grid cell (1), this does not happen due to its high mean altitude (3,699 m a.s.l), yielding snow bands with similar altitudes and, therefore, a similar timing of simulated snow accumulation and melt. During WY 2012 (dry), the alternative model configurations also provide less average SWE than the benchmark model, with specific effects on simulated accumulation and melt events. For example, the 1000-m configuration in grid cell (1) yields the largest melt rates before October, although it provides the highest SWE compared to the other configurations; in grid cell (2), a precipitation event at the end of July/2012 produces snow accumulation only if elevation bands are considered, even though it gets quickly melted; in grid cell (3), the alternative configurations provide less maximum SWE (~20 mm in mid-June) than the benchmark model, despite they generate earlier (almost two weeks) snow accumulation and extend the snow season for more than a week in some cases. Interestingly, although alternative model configurations yield less SWE in

grid cell (1) during WY 2012, lower and earlier snowmelt is obtained compared to the benchmark model, which provides fast, step-like responses.

For the albedo, the largest differences in grid cell (1) are observed in the dry period, especially during the melt season (after September). Around the same date, cumulative sublimation from the alternative configurations begins to depart from the benchmark model results.



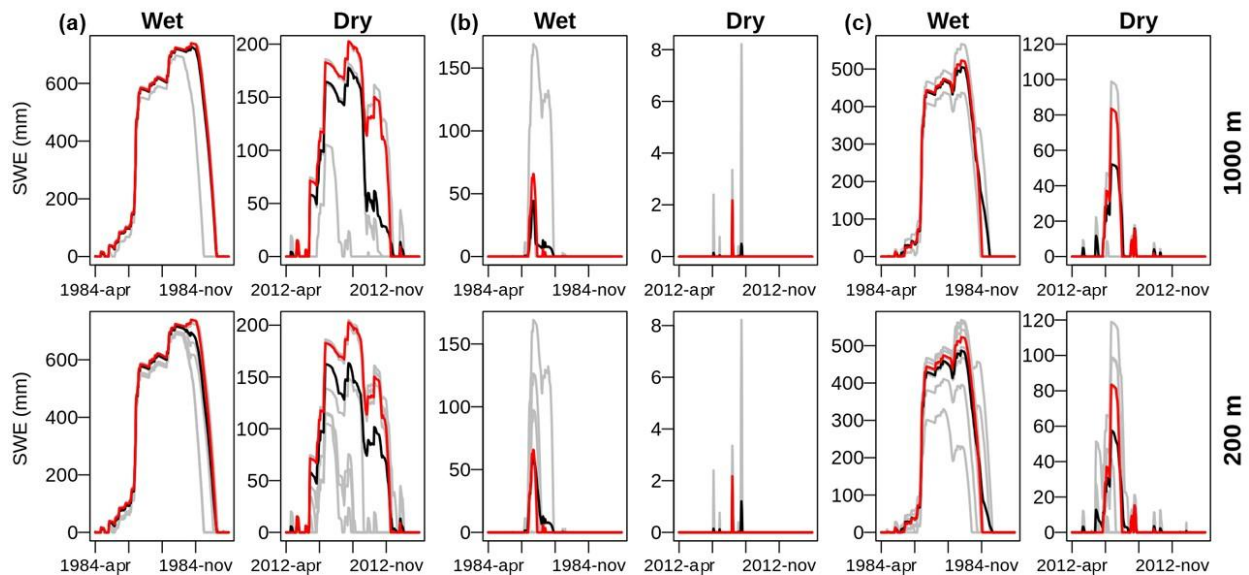
**Figure 8.** Simulated time series of daily SWE, albedo and the cumulative sublimation and cumulative snowmelt for the benchmark model and the alternative model configurations, for the selected grid cells (panels (a), (b) and (c) correspond to grid cells (1), (2) and (3) in Figure 3). Each column displays results for a snow season belonging to a wet (WY 1984) and a dry (WY 2012) water year.

Figure 9 displays time series of daily SWE simulated by individual elevation bands in grid cells (1), (2) and (3) (Figure 3a, 3b, and 3c respectively), using 1000-m (top panel) and 200-m (bottom panel) configurations. It can be noted that differences between the benchmark model (red lines) and the spatial average of alternative configurations (black lines) are attributed to the low accumulation in low-elevation bands (gray lines). The comparison between 1000-m and 200-m simulations shows that adding more elevation bands enhances differences with the benchmark model; for example, the 1000-m (200-m) configuration yields 25 (39) mm less peak SWE than the benchmark in grid cell (1) during the dry period (Figure 9a). Further, the 200-m configuration yields larger seasonally-averaged SWE than the 1000-m configuration due to more snow accumulation at high elevations. Increasing the vertical resolution affects the magnitude of simulated SWE, with higher values in October 2012 using the 200-m configuration (Figure 9a,



dry); indeed, the latter configuration provides a  $\sim 50$  mm reduction in October 20 SWE compared to the benchmark model, while the 1000-m configuration reduces SWE for more than 80 mm the same day. This reveals another interesting feature: despite some high-elevation bands accumulating more SWE than the benchmark model (see gray lines above the red line), this is not translated into increased spatially averaged SWE, due to their low contributing area.

In the low-elevation grid cell (Figure 9b), adding elevation bands yields a longer snow season, and the 200-m configuration enables more snow accumulation (compared to 1000-m), getting closer to the benchmark model results. Finally, the simulations for both (the 200-m) configurations during WY 1984 (WY 2012, after September) in grid cell (3) (Figure 9c) show that adding higher elevation bands can delay the occurrence of grid cell averaged snowmelt events. The highest elevation bands start accumulating snow earlier during WY 2012, compared to the benchmark simulation.

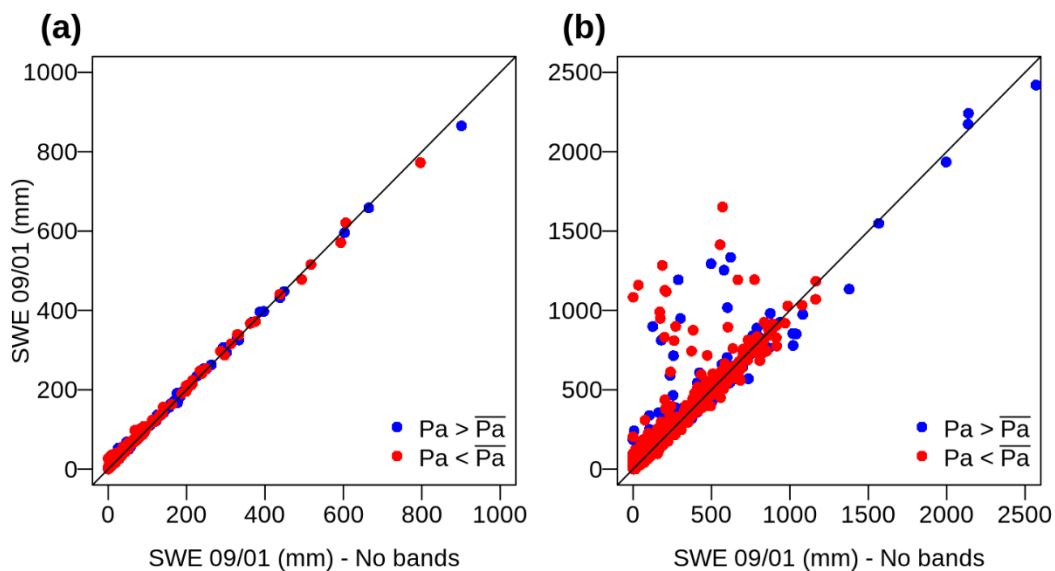


**Figure 9.** Comparison between simulated time series of daily SWE at the grid cell scale (i.e.,  $0.05^\circ$ ) using the benchmark model (red line), vs. an alternative model configuration (black line) with elevation bands ( $\Delta z = 1000$  m, top panel; and  $\Delta z = 200$  m, bottom panels) for selected grid cells (panels (a), (b) and (c) correspond to grid cells (1), (2) and (3) in Figure 3, respectively). In each panel, the gray lines show daily SWE simulated at each elevation band contained in the grid cell of interest. Each column displays results for a snow season belonging to a wet (WY 1984) and a dry (WY 2012) water year.

#### 4.4 Identification of sensitive grid cells

The results in Figure 7 and Figures S7-S8-S9 show that adding elevation bands may have large effects on simulated SWE 09/01 in some grid cells, introducing considerable intra-catchment variability. Nevertheless, this variability compensates in such a way that implementing elevation bands yields smaller (or negligible) effects at the basin scale (Figure 10a), compared to the grid cell scale ( $0.05^\circ$ ) used here (Figure 10b). Hence, we now turn our attention to the question: where does the implementation of elevation bands make a larger difference in simulated SWE? To seek

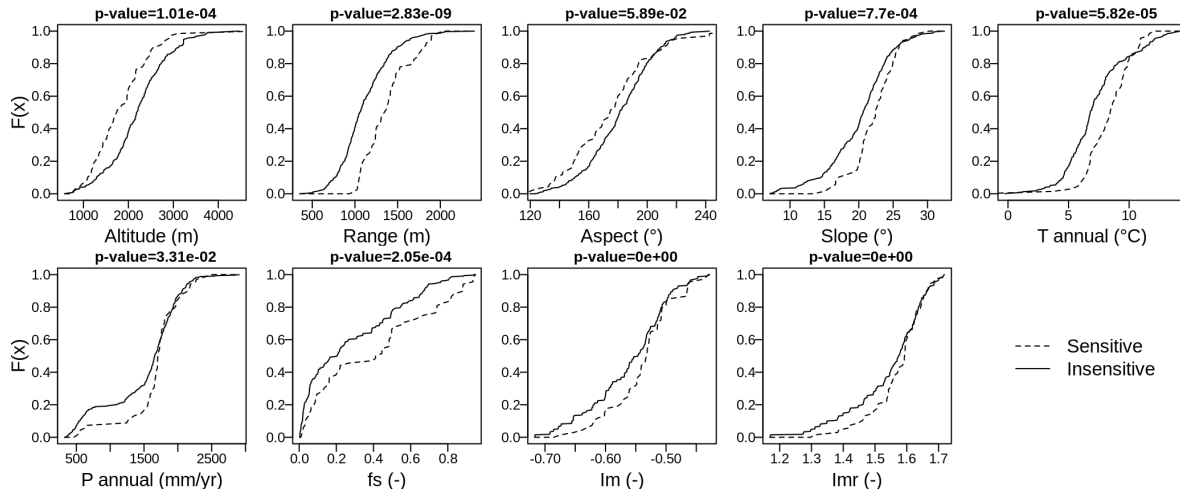
for answers, we examine discrepancies in CDFs of nine topographic and climate attributes (defined in section 3.3.3) between sensitive and insensitive grid cells (Figure 11). The results show that sensitive grid cells have lower mean elevations (median of 1,700 m a.s.l.), larger elevation ranges and average slope, and smaller aspect in the range 120-240 (NW-SW) than insensitive ones. Further, sensitive grid cells show higher mean annual temperatures (median around 8°C compared to 6°C from insensitive grid cells), mean annual precipitation mostly over 1000 mm/yr (90% of sensitive grid cells), and a considerable fraction of precipitation falling as snowfall (the median  $f_s$  value of sensitive grid cells is 0.41, versus a median of 0.20 for insensitive grid cells). The annual average moisture index ( $I_m$ ) and the moisture index seasonality ( $I_{mr}$ ) are larger in sensitive grid cells, indicating more humid conditions and more pronounced intra-annual variations in meteorological conditions, switching from fully arid to fully saturated.



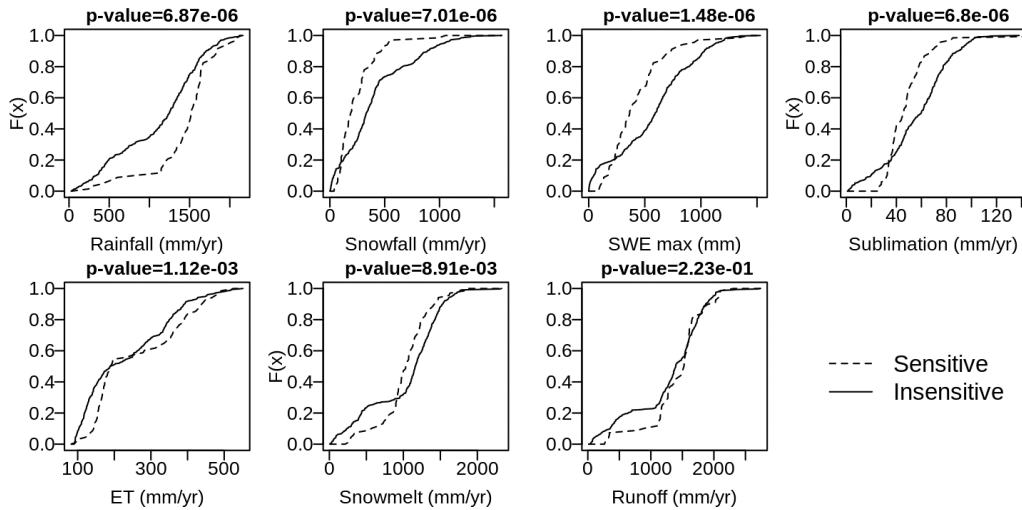
**Figure 10.** Simulated SWE 09/01 using 200-m elevation bands vs. the same variable obtained with the benchmark model at the (a) catchment scale, and (b) individual 0.05° grid cells. Each dot indicates results for a specific combination of water year and spatial unit, and each panel comprises results from all the grid cells contained in the nine case study basins. Results are stratified for dry (red) and wet (blue) water years, defined using the mean annual precipitation ( $\bar{P}_a$ ) for the climatological period as threshold.

Figure 12 displays the CDFs of states and fluxes simulated with 200-m elevation bands in sensitive and insensitive grid cells, showing larger rainfall amounts in sensitive grid cells (median of ~1500 mm/yr) compared to insensitive grid cells (median ~1250 mm/yr); conversely, smaller snowfall amounts (median ~190 mm/yr) are seen in sensitive grid cells compared to insensitive grid cells (median ~330 mm/yr). Accordingly, lower values of maximum SWE are reached in sensitive grid cells (median ~370 mm) compared to insensitive grid cells (median ~590 mm/yr). This behavior is expected given the relatively lower mean elevation of sensitive grid cells (Figure 11). The results for annual snowmelt show large differences in the shape of the CDFs, similar to annual precipitation behavior (Figure 11). The sublimation of sensitive grid cells is higher (median ~60 mm/yr) compared to insensitive grid cells (median ~45 mm/yr), and the shapes of the CDFs are similar to those of maximum SWE. Annual runoff discrepancies between sensitive and

insensitive grid cells are only noticeable for values smaller than 1600 mm/yr, with a relatively larger p-value. Finally, we do not find considerable ET differences between sensitive and insensitive grid cells.



**Figure 11:** CDFs of selected topographic and hydroclimatic attributes for sensitive vs. insensitive grid cells. Aspect values of 180° (90°) represent west (north) facing grid cells. We identify grid cells as sensitive if differences in simulated SWE 09/01 with respect to the benchmark model are larger than 10% for >50% of water years in the climatological period. The p-value is obtained from applying the Kolmogorov-Smirnov test between sensitive and insensitive groups. The results were obtained using the 200-m configuration.



**Figure 12:** Same as in Figure 11, but for model states and fluxes.

## 5 Discussion

The results presented in this paper unveil several implications that the delineation of elevation bands may have on hydrological characterizations, including streamflow performance metrics. Indeed, the KGE results for daily and monthly streamflow (Table 4) do not differ considerably among the model configurations tested here. The maximum KGE improvement provided by alternative model configurations (compared to the benchmark) is  $\Delta KGE = 0.03$  for

the Mapocho and Palos River basins, which cannot be considered an improvement in streamflow simulations due to the inclusion of snow bands (Clark et al., 2021). These small changes suggest a form of model-structure-equifinality for KGE (Khatami et al., 2019), since spatial heterogeneities arising from different modeling alternatives compensate to produce very similar values for the same performance metric applied at the catchment scale. This is not observed, however, when analyzing the bias in the FDC mid-segment slope (%BiasFMS). For Las Leñas and Palos River basins, the bias reductions (100-m – benchmark) are 8.2% and 6.4% respectively. A reduction for the same metric is obtained in the remaining basins when comparing the 100-m configuration with the benchmark, excepting the Arrayán River basin, where the bias increases by 2.3%. For the FDC low-segment volume (%BiasFLV), small variations (<1.1%) are obtained.

Despite the little differences among alternative configurations for KGE (and its components) and NSE, we found notable discrepancies in simulated basin-averaged variables, and spatial differences in rainfall, snowfall, SWE 09/01, sublimation, ET, snowmelt and runoff compared to the benchmark model (Table 4). In general, smaller variations in simulated hydrological variables are obtained as more elevation bands are added, especially beyond a 200-m vertical resolution, which agrees with past studies (e.g., Essery, 2003; Pradhanang et al., 2011; Bhatta et al., 2019). Interestingly, the direction (i.e., sign) of variations introduced by elevation bands (compared to the benchmark) is not the same for all catchments and climate conditions (i.e., wet/dry) of the analysis period.

As expected, simulated processes (i.e., precipitation partitioning into snowfall and rainfall, daily SWE) vary when vertical heterogeneity in air temperature is included, and the effects generally increase with vertical resolution. Such heterogeneity causes differences in snow accumulation across elevation bands, decreasing spatially-averaged peak SWE in each grid cell and delaying snow cover depletion (Figure 9). This aligns well with the findings of Essery (2003), who concluded that the aggregated model (equivalent to our benchmark model) was unable to represent winter melt at low elevations and delayed spring melt at high elevations. Other studies have also highlighted the role of subgrid heterogeneity for more realistic SWE calculations, and therefore for improved snowmelt estimates (e.g., Clark et al., 2011; DeBeer & Pomeroy, 2017). Our results also show that low elevation bands accumulate less SWE and melt earlier, in agreement with observations reported by Tong et al. (2008) for a watershed in western Canada, while the highest elevation bands yield lower melt rates, reducing the snow cover depletion rate (i.e., snow lasts longer). Such differences can be explained by changes in the energy balance (specifically, sensible and latent heat fluxes, Figures S15-S23) since, in our configuration, precipitation is spatially uniform in each grid cell with all model configurations.

A novel contribution of our study is the identification of topographic and climatic controls defining where it is more important to incorporate elevation bands. Our results clearly demonstrate that topographic attributes play a key role, including elevation range, and spatially-averaged elevation and slope. Although we did not find statistically significant differences (i.e.,  $p$ -value > 5%) in terms of aspect between insensitive and sensitive grid cells, the sensitive grid cells group was found to follow a northern orientation. This connection between low elevation and aspect aligns well with the findings of Helfricht et al. (2012), who examined LiDAR observations acquired at the Upper Rofen valley in Austria, concluding that south-facing (equivalent to north-facing in the Southern Hemisphere) exposed slopes at the lowest elevation bands remain almost snow free at the end of 2001, 2002 and 2008 accumulation periods, due to high radiation loads.



A key limitation of this study is that subgrid variability in precipitation was not incorporated (Pradhanang et al., 2011; Grusson et al., 2015), focusing only on air temperature. Hence, future work could expand these analyses to account for orographic controls on precipitation, as well as incoming radiation fluxes or other meteorological forcings, such as wind speed. Because the strategy to delineate snow bands should prioritize a proper representation of SWE at those altitudes with the largest areas, showing high snow accumulation (Helfricht et al., 2012), the effectiveness of irregular vertical discretizations could be tested to emphasize the importance of such areas. Additionally, it would be useful to assess the effects of different elevation band configurations on streamflow forecasts or projected climate change impacts on hydrological variables, including case studies from other snow climates (as in Raleigh et al., 2015) and even simpler (e.g., conceptual, bucket style) hydrologic models.

## 6 Conclusions

We have examined the hydrological implications of representing subgrid variability through elevation bands in nine basins located along the western slopes of the Andes Cordillera. Specifically, we implemented five alternative model configurations in the VIC macro-scale hydrological model, with elevation bands of 1000, 750, 500, 200 and 100 m interval to distribute air temperature, and compared their results against a benchmark model (i.e., model without elevation bands) in terms of streamflow simulations, mean annual fluxes and SWE 09/01, and daily SWE simulations in a suite of grid cells located across the Mapocho River basin. Finally, we analyzed possible physical and climatic characteristics that define those grid cells where elevation bands are more impactful on SWE estimates. The results show that, although the incorporation of elevation bands does not appreciably affect model performance in terms of the Kling-Gupta efficiency for daily and monthly streamflow, it does affect other fluxes and SWE at the catchment scale and the intra-basin variability of simulated variables, suggesting a form of model-structure-equifinality. Other findings are as follows:

- Elevation bands yield larger effects in the partitioning of precipitation into rainfall and snowfall, for both catchment and grid cell scales during the wet period (WYs 1982-1986) compared to the dry period. Additionally, differences in ET and runoff between the alternative model configurations and the benchmark are also more pronounced during the wet period, although not as evident as the case of rainfall and snowfall. On the other hand, impacts of vertical discretization on SWE 09/01 are comparatively more relevant during dry periods.
- Adding elevation bands generally yields less basin-averaged snowmelt, and more (less) catchment-scale sublimation across water-limited (energy-limited) basins.
- The magnitude of variations in simulated hydrological variables induced by elevation bands is not proportional to the vertical discretization or number of elevation bands adopted.
- Adding elevation bands affects the duration of snow cover with the highest bands holding snow for a longer period, and yields earlier snow accumulation during the water year compared to the benchmark model.
- SWE 09/01 is generally more affected by elevation bands in grid cells with relatively lower mean altitude, elevation ranges  $>1000$  m, steep slopes ( $>15^\circ$ ) and annual precipitation amounts  $<1000$  mm with larger intra-annual variations in wetness conditions.

## Acknowledgments

This research was partially supported by the supercomputing infrastructure of the NLHPC (ECM-02). Pablo A. Mendoza received support from Fondecyt Project 11200142 and CONICYT/PIA Project AFB180004. Álvaro Ayala is supported by Fondecyt Postdoctoral Project 3190732. The authors thank Ximena Vargas for her suggestions on earlier versions of this manuscript.

## References

- Abbaspour, K. C., Yang, J., Maximov, I., Siber, R., Bogner, K., Mieleitner, J., et al. (2007). Modelling hydrology and water quality in the pre-alpine/alpine Thur watershed using SWAT. *Journal of Hydrology*, 333(2–4), 413–430. <https://doi.org/10.1016/j.jhydrol.2006.09.014>
- Abdulla, F. A., Lettenmaier, D. P., Wood, E. F., & Smith, J. A. (1996). Application of a macroscale hydrologic model to estimate the water balance of the Arkansas-Red River Basin. *Journal of Geophysical Research: Atmospheres*, 101(D3), 7449–7459. <https://doi.org/10.1029/95JD02416>
- Addor, N., & Melsen, L. A. (2019). Legacy, Rather Than Adequacy, Drives the Selection of Hydrological Models. *Water Resources Research*, 55(1), 378–390. <https://doi.org/10.1029/2018WR022958>
- Aguayo, R., León-Muñoz, J., Garreaud, R., & Montecinos, A. (2021). Hydrological droughts in the southern Andes (40–45°S) from an ensemble experiment using CMIP5 and CMIP6 models. *Scientific Reports*, 11(1), 1–16. <https://doi.org/10.1038/s41598-021-84807-4>
- Alvarez-Garretón, C., Mendoza, P. A., Pablo Boisier, J., Addor, N., Galleguillos, M., Zambrano-Bigiarini, M., et al. (2018). The CAMELS-CL dataset: Catchment attributes and meteorology for large sample studies-Chile dataset. *Hydrology and Earth System Sciences*, 22(11), 5817–5846. <https://doi.org/10.5194/hess-22-5817-2018>
- Andreadis, K. M., & Lettenmaier, D. P. (2006). Assimilating remotely sensed snow observations into a macroscale hydrology model. *Advances in Water Resources*, 29(6), 872–886. <https://doi.org/10.1016/j.advwatres.2005.08.004>
- Andreadis, K. M., Storck, P., & Lettenmaier, D. P. (2009). Modeling snow accumulation and ablation processes in forested environments. *Water Resources Research*, 45, W05429. <https://doi.org/10.1029/2008WR007042>
- Arola, A., & Lettenmaier, D. P. (1996). Effects of Subgrid Spatial Heterogeneity on GCM-Scale Land Surface Energy and Moisture Fluxes. *Journal of Climate*, 9(6), 1339–1349. [https://doi.org/10.1175/1520-0442\(1996\)009<1339:EOSSHO>2.0.CO;2](https://doi.org/10.1175/1520-0442(1996)009<1339:EOSSHO>2.0.CO;2)
- Arora, M., Singh, P., Goel, N. K., & Singh, R. D. (2008). Climate variability influences on hydrological responses of a large himalayan basin. *Water Resources Management*, 22(10), 1461–1475. <https://doi.org/10.1007/s11269-007-9237-1>
- Bajracharya, A. R., Bajracharya, S. R., Shrestha, A. B., & Maharjan, S. B. (2018). Climate change impact assessment on the hydrological regime of the Kaligandaki Basin, Nepal. *Science of the Total Environment*, 625, 837–848. <https://doi.org/10.1016/j.scitotenv.2017.12.332>
- Bandaragoda, C., Tarboton, D. G., & Woods, R. A. (2004). Application of TOPNET in the distributed model intercomparison project. *Journal of Hydrology*, 298(1–4), 178–201. <https://doi.org/10.1016/j.jhydrol.2004.03.038>
- Barnett, T. P., Adam, J. C., & Lettenmaier, D. P. (2005). Potential impacts of a warming climate on water availability in snow-dominated regions. *Nature*, 438(7066), 303–9. <https://doi.org/10.1038/nature04141>

- Beck, H. E., Pan, M., Lin, P., Seibert, J., van Dijk, A. I. J. M., & Wood, E. F. (2020). Global Fully Distributed Parameter Regionalization Based on Observed Streamflow From 4,229 Headwater Catchments. *Journal of Geophysical Research: Atmospheres*, 125(17). <https://doi.org/10.1029/2019JD031485>
- Bhatta, B., Shrestha, S., Shrestha, P. K., & Talchabhadel, R. (2019). Evaluation and application of a SWAT model to assess the climate change impact on the hydrology of the Himalayan River Basin. *Catena*, 181(June), 104082. <https://doi.org/10.1016/j.catena.2019.104082>
- Boisier, J. P., Alvarez-Garretón, C., Cepeda, J., Osses, A., Vásquez, N., & Rondanelli, R. (2018, April). CR2MET: A high-resolution precipitation and temperature dataset for hydroclimatic research in Chile. In *EGU General Assembly Conference Abstracts* (p. 19739).
- C3S, & Copernicus Climate Change Service (C3S). (2017). ERA5: Fifth generation of ECMWF atmospheric reanalyses of the global climate. Retrieved January 20, 2018, from <https://cds.climate.copernicus.eu/cdsapp#!/home>
- Cherkauer, K. A., & Lettenmaier, D. P. (2003). Simulation of spatial variability in snow and frozen soil. *Journal of Geophysical Research*, 108(D22), 8858. <https://doi.org/10.1029/2003JD003575>
- Clark, M. P., Hendrikx, J., Slater, A. G., Kavetski, D., Anderson, B., Cullen, N. J., et al. (2011). Representing spatial variability of snow water equivalent in hydrologic and land-surface models: A review. *Water Resources Research*, 47, W07539. <https://doi.org/10.1029/2011WR010745>
- Clark, M. P., Nijssen, B., & Luce, C. H. (2017). An analytical test case for snow models. *Water Resources Research*, 53(1), 909–922. <https://doi.org/10.1002/2016WR019672>
- Clark, M. P., Vogel, R. M., Lamontagne, J. R., Mizukami, N., Knoben, W. J. M., Tang, G., et al. (2021). The Abuse of Popular Performance Metrics in Hydrologic Modeling. *Water Resources Research*, 57(9), 1–16. <https://doi.org/10.1029/2020WR029001>
- DeBeer, C. M., & Pomeroy, J. W. (2017). Influence of snowpack and melt energy heterogeneity on snow cover depletion and snowmelt runoff simulation in a cold mountain environment. *Journal of Hydrology*, 553, 199–213. <https://doi.org/10.1016/j.jhydrol.2017.07.051>
- Dee, D. P., Uppala, S. M., Simmons, A. J., Berrisford, P., Poli, P., Kobayashi, S., et al. (2011). The ERA-Interim reanalysis: Configuration and performance of the data assimilation system. *Quarterly Journal of the Royal Meteorological Society*, 137(656), 553–597. <https://doi.org/10.1002/qj.828>
- Demaria, E. M. C., Roundy, J. K., Wi, S., & Palmer, R. N. (2016). The effects of climate change on seasonal snowpack and the hydrology of the Northeastern and Upper Midwest United States. *Journal of Climate*, 29(18), 6527–6541. <https://doi.org/10.1175/JCLI-D-15-0632.1>
- DGA. (2017). *Actualización del balance hídrico nacional, SIT N°417, Ministerio de Obras Públicas, Dirección General de Aguas, División de Estudios y Planificación*. Santiago, Chile.
- DGA. (2018). Aplicación de la metodología de actualización del balance hídrico nacional en las cuencas de las macrozonas norte y centro. SIT N° 435. Realizado por Universidad de Chile y Pontificia Universidad Católica. *Gobierno de Chile Ministerio de Obras Públicas*, 44.
- DGA. (2019a). *Aplicación de la metodología de actualización del balance hídrico nacional en la macrozona sur y parte norte de la macrozona Austral, SIT N° 441*.
- DGA. (2019b). *Aplicación De La Metodología De Actualización Del Balance Hídrico Nacional En La Macrozona Sur Y Parte Norte De La Macrozona Austral. SIT N°441, Ministerio de Obras Públicas, Dirección General de Aguas, Santiago, Chile. Elaborado Por: Universidad de Chile, Facultad de Ciencias Físicas y Matemáticas*.

- Didan, K. (2015). *MOD13Q1 MODIS/Terra Vegetation Indices 16-Day L3 Global 250m SIN Grid V006 [Data set]*. NASA EOSDIS Land Processes DAAC. Accessed from <https://doi.org/10.5067/MODIS/MOD13Q1.006>
- Duan, Q. Y., Gupta, V. K., & Sorooshian, S. (1993). Shuffled complex evolution approach for effective and efficient global minimization. *Journal of Optimization Theory and Applications*, 76(3), 501–521. <https://doi.org/10.1007/BF00939380>
- Essery, R. (2003). Aggregated and distributed modelling of snow cover for a high-latitude basin. *Global and Planetary Change*, 38(1–2), 115–120. [https://doi.org/10.1016/S0921-8181\(03\)00013-4](https://doi.org/10.1016/S0921-8181(03)00013-4)
- Fontaine, T. A., Cruickshank, T. S., Arnold, J. G., & Hotchkiss, R. H. (2002). Development of a snowfall-snowmelt routine for mountainous terrain for the soil water assessment tool (SWAT). *Journal of Hydrology*, 262(1–4), 209–223. [https://doi.org/10.1016/S0022-1694\(02\)00029-X](https://doi.org/10.1016/S0022-1694(02)00029-X)
- Garreaud, R., Alvarez-Garretón, C., Barichivich, J., Pablo Boisier, J., Christie, D., Galleguillos, M., et al. (2017). The 2010–2015 megadrought in central Chile: Impacts on regional hydroclimate and vegetation. *Hydrology and Earth System Sciences*, 21(12), 6307–6327. <https://doi.org/10.5194/hess-21-6307-2017>
- Garreaud, R., Boisier, J. P. P., Rondanelli, R., Montecinos, A., Sepúlveda, H. H. H., & Veloso-Aguila, D. (2019). The Central Chile Mega Drought (2010–2018): A climate dynamics perspective. *International Journal of Climatology*, 40(June), 1–19. <https://doi.org/10.1002/joc.6219>
- Gericke, O. J., & Smithers, J. C. (2014). Revue des méthodes d'évaluation du temps de réponse d'un bassin versant pour l'estimation du débit de pointe. *Hydrological Sciences Journal*, 59(11), 1935–1971. <https://doi.org/10.1080/02626667.2013.866712>
- Grusson, Y., Sun, X., Gascoin, S., Sauvage, S., Raghavan, S., Anctil, F., & Sánchez-Pérez, J. M. (2015). Assessing the capability of the SWAT model to simulate snow, snow melt and streamflow dynamics over an alpine watershed. *Journal of Hydrology*, 531, 574–588. <https://doi.org/10.1016/j.jhydrol.2015.10.070>
- Gupta, H. V., Kling, H., Yilmaz, K. K., & Martinez, G. F. (2009). Decomposition of the mean squared error and NSE performance criteria: Implications for improving hydrological modelling. *Journal of Hydrology*, 377(1–2), 80–91. <https://doi.org/10.1016/j.jhydrol.2009.08.003>
- Habets, F., Etchevers, P., Golaz, C., Leblois, E., Ledoux, E., Martin, E., et al. (1999). Simulation of the water budget and the river flows of the Rhone basin. *Journal of Geophysical Research: Atmospheres*, 104(D24), 31145–31172. <https://doi.org/10.1029/1999JD901008>
- Haddeland, I., Matheussen, B. V., & Lettenmaier, D. P. (2002). Influence of spatial resolution on simulated streamflow in a macroscale hydrologic model. *Water Resources Research*, 38(7), 29-1-29–10. <https://doi.org/10.1029/2001WR000854>
- Hartman, M. D., Baron, J. S., Lammers, R. B., Cline, D. W., Band, L. E., Liston, G. E., & Tague, C. (1999). Simulations of snow distribution and hydrology in a mountain basin. *Water Resources Research*, 35(5), 1587–1603. <https://doi.org/10.1029/1998WR900096>
- Helfricht, K., Schöber, J., Seiser, B., Fischer, A., Stötter, J., & Kuhn, M. (2012). Snow accumulation of a high alpine catchment derived from LiDAR measurements. *Advances in Geosciences*, 32, 31–39. <https://doi.org/10.5194/adgeo-32-31-2012>
- IPCC. (2021). Assessment Report 6 Climate Change 2021: The Physical Science Basis.
- Khatami, S., Peel, M. C., Peterson, T. J., & Western, A. W. (2019). Equifinality and Flux Mapping:

- A New Approach to Model Evaluation and Process Representation Under Uncertainty. *Water Resources Research*, 55(11), 8922–8941. <https://doi.org/10.1029/2018WR023750>
- Knoben, W. J. M., Woods, R. A., & Freer, J. E. (2018). A Quantitative Hydrological Climate Classification Evaluated With Independent Streamflow Data. *Water Resources Research*, 54(7), 5088–5109. <https://doi.org/10.1029/2018WR022913>
- Lehning, M., Völksch, I., Gustafsson, D., Nguyen, T. A., Stähli, M., & Zappa, M. (2006). ALPINE3D: a detailed model of mountain surface processes and its application to snow hydrology. *Hydrological Processes*, 20(10), 2111–2128. <https://doi.org/10.1002/hyp.6204>
- Li, D., Wrzesien, M. L., Durand, M., Adam, J., & Lettenmaier, D. P. (2017). How much runoff originates as snow in the western United States, and how will that change in the future? *Geophysical Research Letters*. <https://doi.org/10.1002/2017GL073551>
- Liang, X., Lettenmaier, D. P., Wood, E. F., & Burges, S. J. (1994). A simple hydrologically based model of land surface water and energy fluxes for general circulation models. *Journal of Geophysical Research*, 99(D7), 14,415–14,428. <https://doi.org/10.1029/94jd00483>
- Liang, X., Wood, E. F., & Lettenmaier, D. P. (1996). Surface soil moisture parameterization of the VIC-2L model: Evaluation and modification. *Global and Planetary Change*, 13(1–4), 195–206. [https://doi.org/10.1016/0921-8181\(95\)00046-1](https://doi.org/10.1016/0921-8181(95)00046-1)
- Liston, G., & Sturm, M. (1998). A snow-transport model for complex terrain. *Journal of Glaciology*.
- López-Moreno, J. I., Pomeroy, J. W., Revuelto, J., & Vicente-Serrano, S. M. (2013). Response of snow processes to climate change: spatial variability in a small basin in the Spanish Pyrenees. *Hydrological Processes*, 27(18), 2637–2650. <https://doi.org/10.1002/hyp.9408>
- Markstrom, S. L., Niswonger, R. G., Regan, R. S., Prudic, D. E., & Barlow, P. M. (2008). *GSFLOW — Coupled Ground-Water and Surface-Water Flow Model Based on the Integration of the Precipitation-Runoff Modeling System ( PRMS ) and the Modular Ground-Water Flow Model ( MODFLOW-2005 )*. *Methods*.
- Masiokas, M. H., Rabatel, A., Rivera, A., Ruiz, L., Pitte, P., Ceballos, J. L., et al. (2020). A Review of the Current State and Recent Changes of the Andean Cryosphere. *Frontiers in Earth Science*, 8(June), 1–27. <https://doi.org/10.3389/feart.2020.00099>
- Melsen, L. A., Teuling, A. J., Torfs, P. J. J. F., Zappa, M., Mizukami, N., Mendoza, P. A., et al. (2019). Subjective modeling decisions can significantly impact the simulation of flood and drought events. *Journal of Hydrology*, 568(November 2018), 1093–1104. <https://doi.org/10.1016/j.jhydrol.2018.11.046>
- Mendoza, P. A., Rajagopalan, B., Clark, M. P., Cortés, G., & McPhee, J. (2014). A robust multimodel framework for ensemble seasonal hydroclimatic forecasts. *Water Resources Research*, 50(7), 6030–6052. <https://doi.org/10.1002/2014WR015426>
- Mendoza, P. A., Clark, M. P., Mizukami, N., Gutmann, E. D., Arnold, J. R., Brekke, L. D., & Rajagopalan, B. (2016). How do hydrologic modeling decisions affect the portrayal of climate change impacts? *Hydrological Processes*, 30(7), 1071–1095. <https://doi.org/10.1002/hyp.10684>
- Mendoza, P. A., Shaw, T. E., McPhee, J., Musselman, K. N., Revuelto, J., & MacDonell, S. (2020). Spatial Distribution and Scaling Properties of Lidar-Derived Snow Depth in the Extratropical Andes. *Water Resources Research*, 56(12). <https://doi.org/10.1029/2020WR028480>
- Mizukami, N., P. Clark, M., G. Slater, A., D. Brekke, L., M. Elsner, M., R. Arnold, J., et al. (2014). Hydrologic Implications of Different Large-Scale Meteorological Model Forcing Datasets in Mountainous Regions. *Journal of Hydrometeorology*, 15(1), 474–488.

- https://doi.org/10.1175/JHM-D-13-036.1
- Mizukami, N., Clark, M. P., Gutmann, E. D., Mendoza, P. A., Newman, A. J., Nijssen, B., et al. (2016). Implications of the Methodological Choices for Hydrologic Portrayals of Climate Change over the Contiguous United States: Statistically Downscaled Forcing Data and Hydrologic Models. *Journal of Hydrometeorology*, 17(1), 73–98. https://doi.org/10.1175/JHM-D-14-0187.1
- Myneni, R., Knyazikhin, Y., Park, T. (2015). *MCD15A2H MODIS/Terra+Aqua Leaf Area Index/FPAR 8-day L4 Global 500m SIN Grid V006 [Data set]*. NASA EOSDIS Land Processes DAAC. Accessed from https://doi.org/10.5067/MODIS/MCD15A2H.006
- NASA/METI/AIST/Japan Spacesystems and U.S./Japan ASTER Science Team (2001). *ASTER DEM Product [Version 3]*. NASA EOSDIS Land Processes DAAC. Accessed 2021-05-16 from https://doi.org/10.5067/ASTER/AST14DEM.003
- Nash, J., & Sutcliffe, J. (1970). River flow forecasting through conceptual models part I - A discussion of principles. *Journal of Hydrology*, 10(3), 282–290. https://doi.org/10.1016/0022-1694(70)90255-6
- Newman, A. J., Clark, M. P., Winstral, A., Marks, D., & Seyfried, M. (2014). The Use of Similarity Concepts to Represent Sub-grid Variability in Land-Surface Models: Case Study in a Snowmelt Dominated Watershed. *Journal of Hydrometeorology*, In Press. https://doi.org/10.1175/JHM-D-13-038.1
- Newman, A. J., Mizukami, N., Clark, M. P., Wood, A. W., Nijssen, B., & Nearing, G. (2017). Benchmarking of a physically based hydrologic model. *Journal of Hydrometeorology*, 18(8), 2215–2225. https://doi.org/10.1175/JHM-D-16-0284.1
- Pradhanang, S. M., Anandhi, A., Mukundan, R., Zion, M. S., Pierson, D. C., Schneiderman, E. M., et al. (2011). Application of SWAT model to assess snowpack development and streamflow in the Cannonsville watershed, New York, USA. *Hydrological Processes*, 25(21), 3268–3277. https://doi.org/10.1002/hyp.8171
- Prata, A. J. (1996). A new long-wave formula for estimating downward clear-sky radiation at the surface. *Quarterly Journal of the Royal Meteorological Society*, 122(533), 1127–1151. https://doi.org/10.1002/qj.49712253306
- Quintana, J., & Aceituno, P. (2012). Changes in the rainfall regime along the extratropical west coast of South America (Chile): 30–43° S. *Atmósfera*, 25(1), 1–22.
- Ragetti, S., Cortés, G., McPhee, J., & Pellicciotti, F. (2014). An evaluation of approaches for modelling hydrological processes in high-elevation, glacierized Andean watersheds. *Hydrological Processes*, 28(23), 5674–5695. https://doi.org/10.1002/hyp.10055
- Raleigh, M. S., Lundquist, J. D., & Clark, M. P. (2015). Exploring the impact of forcing error characteristics on physically based snow simulations within a global sensitivity analysis framework. *Hydrology and Earth System Sciences*, 19(7), 3153–3179. https://doi.org/10.5194/hess-19-3153-2015
- Rasmussen, R., Ikeda, K., Liu, C., Gochis, D., Clark, M., Dai, A., et al. (2014). Climate Change Impacts on the Water Balance of the Colorado Headwaters: High-Resolution Regional Climate Model Simulations. *Journal of Hydrometeorology*, 15(3), 1091–1116. https://doi.org/10.1175/JHM-D-13-0118.1
- Schneider, D., & Molotch, N. P. (2016). Real-time estimation of snow water equivalent in the Upper Colorado River Basin using MODIS-based SWE Reconstructions and SNOTEL data. *Water Resources Research*, 52(10), 7892–7910. https://doi.org/10.1002/2016WR019067
- Sepúlveda, U. M., Mendoza, P. A., Mizukami, N., & Newman, A. J. (2021). Revisiting parameter

- sensitivities in the Variable Infiltration Capacity model. *Hydrology and Earth System Sciences Discussions*, (November), in review. <https://doi.org/https://doi.org/10.5194/hess-2021-550>
- Tong, J., Déry, S., & Jackson, P. (2008). Topographic control of snow distribution in an alpine watershed of western Canada inferred from spatially-filtered MODIS snow products. *Hydrology and Earth System Sciences Discussions*, 5(4), 2347–2371. <https://doi.org/10.5194/hessd-5-2347-2008>
- Vargas, X., Gómez, T., Ahumada, F., Rubio, E., Cartes, M., & Gibbs, M. (2013). Water availability in a mountainous Andean watershed under CMIP5 climate change scenarios. *IAHS-AISH Proceedings and Reports*, 360(July), 33–38.
- Vásquez, N., Cepeda, J., Gómez, T., Mendoza, P. A., Lagos, M., Boisier, J. P., et al. (2021). Catchment-Scale Natural Water Balance in Chile. In *Water Resources of Chile* (pp. 189–208). [https://doi.org/10.1007/978-3-030-56901-3\\_9](https://doi.org/10.1007/978-3-030-56901-3_9)
- Vicuña, S., Garreaud, R. D., & McPhee, J. (2011). Climate change impacts on the hydrology of a snowmelt driven basin in semiarid Chile. *Climatic Change*, 105(3–4), 469–488. <https://doi.org/10.1007/s10584-010-9888-4>
- Vicuña, S., Vargas, X., Boisier, J. P., Mendoza, P. A., Gómez, T., Vásquez, N., & Cepeda, J. (2021). Impacts of Climate Change on Water Resources in Chile. In *Water Resources of Chile* (Vol. 13, pp. 347–363). [https://doi.org/10.1007/978-3-030-56901-3\\_19](https://doi.org/10.1007/978-3-030-56901-3_19)
- Voordendag, A., Réveillet, M., MacDonell, S., & Lhermitte, S. (2021). Snow model comparison to simulate snow depth evolution and sublimation at point scale in the semi-arid Andes of Chile. *Cryosphere*, 15(9), 4241–4259. <https://doi.org/10.5194/tc-15-4241-2021>
- Yilmaz, K. K., Gupta, H. V., & Wagener, T. (2008). A process-based diagnostic approach to model evaluation: Application to the NWS distributed hydrologic model. *Water Resources Research*, 44(9), W09417. <https://doi.org/10.1029/2007WR006716>
- Zhao, Y., Feng, D., Yu, L., Wang, X., Chen, Y., Bai, Y., et al. (2016). Detailed dynamic land cover mapping of Chile: Accuracy improvement by integrating multi-temporal data. *Remote Sensing of Environment*, 183, 170–185. <https://doi.org/10.1016/j.rse.2016.05.016>